


## Visible–near infrared spectral indices for mapping mineralogy and chemistry with OSIRIS-REx

Hannah H. KAPLAN<sup>1</sup><sup>\*</sup>, Victoria E. HAMILTON<sup>1</sup>, Ellen S. HOWELL<sup>2</sup>, F. Scott ANDERSON<sup>1</sup>, M. Antonella BARRUCCI<sup>3</sup>, John BRUCATO<sup>4</sup>, Thomas H. BURBINE<sup>5</sup>, Beth E. CLARK<sup>6</sup>, Ed A. CLOUTIS<sup>7</sup>, Harold C. CONNOLLY JR.<sup>8</sup>, Elisabetta DOTTO<sup>9</sup>, Joshua P. EMERY<sup>10</sup>, Sonia FORNASIER<sup>3,11</sup>, Cateline LANTZ<sup>12</sup>, Lucy F. LIM<sup>13</sup>, Frederic MERLIN<sup>3</sup>, Alice PRAET<sup>3</sup>, Dennis C. REUTER<sup>13</sup>, Scott A. SANDFORD<sup>14</sup>, Amy A. SIMON<sup>13</sup>, Driss TAKIR<sup>15</sup>, and Dante S. LAURETTA<sup>2</sup>

<sup>1</sup>Southwest Research Institute, Boulder, Colorado 80302, USA

<sup>2</sup>Lunar and Planetary Laboratory, University of Arizona, Tucson, Arizona 85721, USA

<sup>3</sup>LESIA, Observatoire de Paris, Université PSL, CNRS, Université de Paris, Sorbonne Université, 5 place Jules Janssen, 92195 Meudon, France

<sup>4</sup>INAF Osservatorio Astrofisico di Arcetri 50125, Firenze, Italy

<sup>5</sup>Mount Holyoke College, South Hadley, Massachusetts 01075, USA

<sup>6</sup>Ithaca College, Ithaca, New York 14850, USA

<sup>7</sup>University of Winnipeg, Winnipeg, Manitoba R3T 2N2, Canada

<sup>8</sup>Rowan University, Glassboro, New Jersey 08028, USA

<sup>9</sup>INAF Osservatorio Astronomico di Roma, 00136 Rome, Italy

<sup>10</sup>Northern Arizona University, Flagstaff, Arizona 86011, USA

<sup>11</sup>Institut Universitaire de France (IUF), 1 rue Descartes, 75231 Paris Cedex 05, France

<sup>12</sup>Institut d'Astrophysique Spatiale, 91440 Orsay, France

<sup>13</sup>NASA Goddard Space Flight Center, Greenbelt, Maryland 20771, USA

<sup>14</sup>NASA Ames Research Center, Moffett Field, California 94035, USA

<sup>15</sup>JETS/ARES, NASA Johnson Space Center, Houston, Texas 77058, USA

\*Corresponding author. E-mail: kaplan@boulder.swri.edu

(Received 03 May 2019; revision accepted 23 January 2020)

---

**Abstract**–The primary objective of the Origins, Spectral Interpretation, Resource Identification, and Security–Regolith Explorer (OSIRIS-REx) mission is to return to Earth a pristine sample of carbonaceous material from the primitive asteroid (101955) Bennu. To support compositional mapping of Bennu as part of sample site selection and characterization, we tested 95 spectral indices on visible to near infrared laboratory reflectance data from minerals and carbonaceous meteorites. Our aim was to determine which indices reliably identify spectral features of interest. Most spectral indices had high positive detection rates when applied to spectra of pure, single-component materials. The meteorite spectra have fewer and weaker absorption features and, as a result, fewer detections with the spectral indices. Indices targeting absorptions at 0.7 and 2.7–3  $\mu\text{m}$ , which are attributable to hydrated minerals, were most successful for the meteorites. Based on these results, we identified a set of 17 indices that are most likely to be useful at Bennu. These indices detect olivines, pyroxenes, carbonates, water/OH-bearing minerals, serpentines, ferric minerals, and organics. Particle size and albedo are known to affect band depth but had a negligible impact on interpretive success with spectral indices. Preliminary analysis of the disk-integrated Bennu spectrum with these indices is consistent with expectations given the observed absorption near 3  $\mu\text{m}$ . Our study prioritizes spectral indices to be used for OSIRIS-REx spectral analysis and mapping and informs the reliability of all index-derived data products, including a science value map for sample site selection.

---

## INTRODUCTION

Two spectrometers on the Origins, Spectral Interpretation, Resource Identification, and Security–Regolith Explorer (OSIRIS-REx) spacecraft will map (101955) Bennu’s surface composition and thermophysical properties before the spacecraft collects and returns a sample of the asteroid. One of these instruments, the OSIRIS-REx Visible and InfraRed Spectrometer (OVIRS), is a point spectrometer that measures reflected light from 0.4 to 4.3  $\mu\text{m}$ , a spectral range that contains features associated with minerals, water, and organics. OVIRS will collect >450,000 spectra (resampled to 1393 channels) at spatial resolutions of  $\sim 20$  m during global spectral mapping and  $\sim 4$  m during reconnaissance mapping (Reuter et al. 2018). We will use spectral indices to reduce the hyperspectral data to single values that direct the science team to regions of interest on Bennu and that can be mapped to evaluate mineral and chemical presence and distribution. This data reduction step is necessary to analyze the large number of spectra collected over the course of the mission. These indices target specific spectral absorptions associated with phases of interest (e.g., organics). The resulting mineral/chemical maps contribute substantially to a science value map that will inform sample site selection.

In advance of OSIRIS-REx’s arrival at Bennu, we collected over 100 spectral indices from the literature, wrote software to apply them to data having OVIRS’s spectral resolution, and tested the indices using laboratory spectra of minerals and meteorites. These tests gauge the fidelity and applicability of each spectral index to materials that are relevant to the surface of Bennu. Here we present a subset of indices expected to be most useful for science and discuss the conditions under which these indices perform best.

## BACKGROUND

Bennu was chosen as the target of the OSIRIS-REx mission for its proximity to Earth and regolith properties (Lauretta et al. 2015). Bennu is a near-Earth object considered dynamically likely to have originated in the Polana-Eulalia inner main-belt families (Walsh et al. 2013; Bottke et al. 2015; Campins et al. 2018; De León et al. 2018). Ground-based visible to near infrared (VIS-NIR) spectra of Bennu exhibit a negative (blue) slope and it is classified as a B-type asteroid in the Bus-DeMeo taxonomy (Clark et al. 2011). B-types are thought to be compositionally primitive and volatile rich, and are sometimes observed to have a 0.7  $\mu\text{m}$  absorption, which is associated with hydrated minerals

(Clark et al. 2010). Spectra of Bennu lack this 0.7  $\mu\text{m}$  absorption. Binzel et al. (2015) observed variation in Bennu’s spectral slope with multiple viewings, which they attributed to particle size variation from regolith accumulation at the equatorial ridge.

Comparison of Bennu’s ground-based spectrum with a database of laboratory spectra suggested that Bennu is spectrally similar to the carbonaceous (C) chondrites, specifically the aqueously altered CI and CM groups (Clark et al. 2011). The CIs and CMs have low reflectance (<10% in the VIS-NIR spectral range) and show great variability in spectral shape, slope, and number of absorptions depending on the degree of alteration, particle size, and viewing geometry (e.g., Johnson and Fanale 1973; Cloutis et al. 2011a, 2011b; Beck et al. 2018). Absorptions associated with hydration ( $\text{H}_2\text{O}$ ) or hydrated minerals ( $\text{OH}^-$ ) are prominent in many of the CI and CM meteorite spectra at 0.7  $\mu\text{m}$  and ubiquitous at 2.7–3  $\mu\text{m}$  (e.g., Hiroi et al. 1996; Beck et al. 2010), and are also observed in B- and C-type asteroids (Vilas and Gaffey 1989; Vilas 1994; Rivkin 2002; Clark et al. 2010; Takir and Emery 2012; Takir et al. 2015). Weaker absorptions due to vibrational modes and overtones in phyllosilicates, carbonates, sulfates, and organics are seen in some laboratory spectra (Cloutis et al. 2011a).

Carbonaceous chondrite mineralogy has been extensively studied (e.g., Tomeoka and Buseck 1988; Zolensky et al. 1993; Lauretta et al. 2000; Bland et al. 2004; Howard et al. 2009, 2015; King et al. 2015). Briefly, anhydrous silicates, such as olivine, pyroxene, and plagioclase, are commonly found in carbonaceous meteorites, with abundances that diminish with progressive aqueous alteration (e.g., McSween 1977; Sheng et al. 1991; Browning et al. 1996; Howard et al. 2015). Phyllosilicates, specifically (Mg, Fe) serpentines and smectitic clay minerals such as saponite, are common products of aqueous processing and make up 75–80% of the volume of some CM and CI meteorites (Howard et al. 2009, 2015; King et al. 2015). CM chondrites contain abundant tochilinite (approximately  $\text{FeS}(\text{Mg,Fe})(\text{OH})_2$ ), an iron sulfide-hydroxide phase. Metals (Fe, Ni) and sulfides are also found in C chondrites (e.g., Abreu and Brearley 2010), although they are unlikely to be observed in VIS-NIR spectra owing to a lack of absorption features. Magnetite, Fe-oxides, and Fe-hydroxides can have a considerable effect on albedo and VIS-NIR absorptions even in low abundances (Cloutis et al. 2011a). Organics contribute up to 5 wt% carbon to these meteorites, typically in an insoluble form with a varied composition (e.g., Alexander et al. 2007, 2017). Carbon can also reside in carbonates (e.g., Alexander et al. 2015).

Table 1. Parameter descriptions: A list of the 95 spectral indices analyzed in this paper (of the 107 total calculated by Spindex), their source, the equation type, the defining wavelengths and constants, and threshold value. Type corresponds to equation numbers in Fig. S1 in supporting information, and those equations, along with the wavelength positions and constants, allow for the spectral index to be calculated on any spectrum.

#	Parameter	Source	Type	Wavelength positions and constants						Thresh.
1	H <sub>2</sub> O @ 1.50 μm	Lebofsky (1980), Hudgins et al. (1993), Mastrapa et al. (2009)	4	1.4	1.5	1.7	0	0	0	0.05
2	H <sub>2</sub> O, OH @ 1.95 μm	Lebofsky (1980), Hudgins et al. (1993), Mastrapa et al. (2009)	2	1.9	1.95	2	0	0	0	0.05
3	H <sub>2</sub> O, OH @ 3 μm	Pelkey et al. (2007)	6	2.21	2.53	3	0	0	0	0.05
4	H <sub>2</sub> O, OH @ 2.95 μm	Moroz et al. (1998)	5	2.7	2.95	3.33	0	0.6	0.4	0.05
5	H <sub>2</sub> O @ 1.51 μm	Pelkey et al. (2007), Mastrapa et al. (2009), Grundy and Schmitt (1998)	1	1.3	1.51	1.695	0	0	0	0.05
6	H <sub>2</sub> O, OH @ 1.93 μm	Pelkey et al. (2007), Mastrapa et al. (2009), Grundy and Schmitt (1998)	8	1.857	1.93	1.935	2.067	0	0	0.05
7	OH @ 2.7 μm	Feaga et al. (2007)	5	2.55	2.7	2.76	0	0.25	0.75	0.05
8	H <sub>2</sub> O @ 3.12 μm (ice)	Pelkey et al. (2007), Merlin et al. (2012)	1	3	3.12	3.25	0	0	0	0.05
9	Aromatic CC, CH @ 2.16 μm	Moroz et al. (1998)	2	2.06	2.16	2.26	0	0	0	0.05
10	CO <sub>2</sub> @ 1.43 μm	Pelkey et al. (2007)	1	1.37	1.43	1.47	0	0	0	0.05
11	CO <sub>2</sub> @ 3.32 μm	Pelkey et al. (2007)	1	3.25	3.32	3.39	0	0	0	0.05
12	DNU—NH @ 2.99 μm	Bossa et al. (2009)	2	2.85	3	3.15	0	0	0	0.05
13	DNU—NH @ 3.43 μm	Gerakines et al. (2012)	2	3.28	3.43	3.58	0	0	0	0.05
14	CO <sub>2</sub> @ 4.25 μm	Feaga et al. (2007)	5	4.18	4.25	4.32	0	0.5	0.5	0.05
15	Spinel group @ 2.1 μm	Cloutis et al. (2004)	2	1.5	2.1	2.7	0	0	0	0.05
16	Fe <sub>3</sub> @ 0.5 μm (ilmenite, magnetite)	Cloutis et al. (2011a, 2011b)	2	0.45	0.5	0.55	0	0	0	0.05
17	Chromite @ 0.58 μm	Cloutis et al. (2004)	2	0.55	0.58	0.61	0	0	0	0.05
18	Chromite @ 0.67 μm	Cloutis et al. (2004)	2	0.64	0.67	0.7	0	0	0	0.05
19	Chromite @ 0.9 μm	Cloutis et al. (2004)	2	0.8	0.9	1	0	0	0	0.05
20	Chromite @ 1.2 μm	Cloutis et al. (2004)	2	1.1	1.2	1.3	0	0	0	0.05
21	Hematite @ 0.9 μm	Cloutis et al. (2004)	9	0.7	0.9	1.2	0	0.6	0.4	0.05
22	Hercynite @ 0.46 μm	Cloutis et al. (2004)	2	0.43	0.46	0.49	0	0	0	0.05
23	Hercynite @ 0.55 μm	Cloutis et al. (2004)	2	0.52	0.55	0.58	0	0	0	0.05
24	Hercynite @ 0.66 μm	Cloutis et al. (2004)	2	0.62	0.66	0.72	0	0	0	0.05
25	Hercynite @ 0.93 μm	Cloutis et al. (2004)	2	0.83	0.93	1.03	0	0	0	0.05
26	Spinel @ 0.54 μm	Cloutis et al. (2004)	2	0.49	0.54	0.59	0	0	0	0.05
27	Gypsum @ 1.45 μm	Cloutis et al. (2006)	4	1.3	1.45	1.7	0	0	0	0.05
28	Gypsum @ 1.49 μm	Cloutis et al. (2006)	2	1.47	1.49	1.51	0	0	0	0.05
29	Gypsum @ 1.53 μm	Cloutis et al. (2006)	2	1.51	1.53	1.55	0	0	0	0.05
30	Epsomite @ 1.45 μm	Cloutis et al. (2006, 2011a, 2011b)	4	1.3	1.45	1.75	0	0	0	0.05
31	Epsomite @ 1.95 μm	Cloutis et al. (2006, 2011a, 2011b)	4	1.8	1.95	2.25	0	0	0	0.05
32	Gypsum @ 1.94 μm	Cloutis et al. (2006)	2	1.84	1.94	2.04	0	0	0	0.05
33	Gypsum @ 1.97 μm	Cloutis et al. (2006)	2	1.95	1.97	1.99	0	0	0	0.05
34	Gypsum @ 2.2 μm	Cloutis et al. (2006)	2	2.1	2.2	2.3	0	0	0	0.05
35	Gypsum @ 1.75 μm	Cloutis et al. (2006)	2	1.7	1.75	1.8	0	0	0	0.05
36	Gypsum @ 1.78 μm	Cloutis et al. (2006)	2	1.75	1.78	1.81	0	0	0	0.05
37	Gypsum @ 2.48 μm	Cloutis et al. (2006)	2	2.4	2.48	2.56	0	0	0	0.05

Table 1. *Continued.* Parameter descriptions: A list of the 95 spectral indices analyzed in this paper (of the 107 total calculated by Spindex), their source, the equation type, the defining wavelengths and constants, and threshold value. Type corresponds to equation numbers in Fig. S1 in supporting information, and those equations, along with the wavelength positions and constants, allow for the spectral index to be calculated on any spectrum.

#	Parameter	Source	Type	Wavelength positions and constants						Thresh.
38	CO @ 3.95 $\mu\text{m}$ (carbonate-calcite)	Pelkey et al. (2007)	10	3.63	3.75	3.95	0	0	0	0.07
39	Pyroxene @ 1.33 $\mu\text{m}$ (LCP)	Pelkey et al. (2007)	11	1.05	1.33	1.815	0	0	0	0.05
40	Pyroxene @ 1.47 $\mu\text{m}$ (HCP)	Pelkey et al. (2007)	11	1.05	1.47	2.067	0	0	0	0.05
41	Pyroxene @ 2.2 $\mu\text{m}$	Ody et al. (2012)	12	1.79	2.15	2.22	2.5	0	0	0.05
42	Olivine @ 1.25 $\mu\text{m}$	King and Ridley (1987)	2	1.2	1.25	1.3	0	0	0	0.05
43	Olivine @ 1.01–1.36 $\mu\text{m}$ (Lo-Fe)	Ody et al. (2012)	13	1.01	1.21	1.36	1.54	1.56	0	1.07
44	Olivine @ 1.01–1.5 $\mu\text{m}$ (Hi-Fe)	Ody et al. (2012)	14	1.01	1.21	1.36	1.5	1.69	1.7	1.07
45	Pyroxene @ 1.084 $\mu\text{m}$ (HCP)	Adams (1974)	1	0.97	1.084	1.148	0	0	0	0.05
46	Pyroxene @ 1.05 $\mu\text{m}$ (wide)	King and Ridley (1987)	2	0.7	1.05	1.4	0	0	0	0.05
47	Pyroxene @ 1.9 $\mu\text{m}$	King and Ridley (1987)	2	1.4	1.9	2.4	0	0	0	0.05
48	Olivine @ 1.05–1.47 $\mu\text{m}$	Pelkey et al. (2007)	15	1.05	1.21	1.33	1.47	1.695	0	0.05
49	Olivine @ 1.418 $\mu\text{m}$	Ody et al. (2012)	16	1.218	1.418	1.818	0	0	0	0.05
50	Fe2-Fe3 @ 0.7 $\mu\text{m}$ (serpentine)	Vilas (1994)	17	0.55	0.701	0.853	0	0	0	0.99
51	Chlorite @ 2.30 $\mu\text{m}$	King and Clark (1989)	0	2.19	2.3	2.41	0	0	0	0.05
52	OH,H <sub>2</sub> O @ 2.85 $\mu\text{m}$	Sunshine et al. (2009), Pelkey et al. (2007)	6	2.21	2.35	3	0	0	0	0.05
53	OH, H <sub>2</sub> O @ 1.93 $\mu\text{m}$	Michalski et al. (2010), Pelkey et al. (2007)	12	1.8	1.93	1.94	2.2	0	0	0.05
54	Al-OH @ 2.2 $\mu\text{m}$	Pelkey et al. (2007)	1	2.14	2.21	2.25	0	0	0	0.05
55	Mg-OH @ 2.29 $\mu\text{m}$	Pelkey et al. (2007)	1	2.25	2.29	2.35	0	0	0	0.05
56	Fe2 @ 0.9 $\mu\text{m}$ (phyllosilicate)	Cloutis et al. (2011a, 2011b)	2	0.8	0.9	1	0	0	0	0.05
57	Fe2 @ 1.1 $\mu\text{m}$ (phyllosilicate)	Cloutis et al. (2011a, 2011b); King and Clark (1989)	2	1	1.1	1.2	0	0	0	0.05
58	Biotite @ 1.30 $\mu\text{m}$	Clark (1999)	3	1	1.3	2.2	0	0	0	0.05
59	Mica @ 2.21 $\mu\text{m}$	Pelkey et al. (2007)	2	2.14	2.21	2.25	0	0	0	0.05
60	Mica @ 2.44 $\mu\text{m}$	Pelkey et al. (2007)	0	2.29	2.44	2.54	0	0	0	0.05
61	DNU—Montmorillonite @ 0.5 $\mu\text{m}$	Pelkey et al. (2007)	0	0.47	0.5	0.57	0	0	0	0.05
62	DNU—Saponite @ 3.4 $\mu\text{m}$	Pelkey et al. (2007)	0	3.324	3.4	3.544	0	0	0	0.05
63	Talc @ 2.38 $\mu\text{m}$	Pelkey et al. (2007)	0	2.34	2.38	2.41	0	0	0	0.05
64	Talc @ 2.49 $\mu\text{m}$	Pelkey et al. (2007)	0	2.41	2.49	2.6	0	0	0	0.05
65	DNU—Talc @ 3.38 $\mu\text{m}$	Pelkey et al. (2007)	0	3.26	3.38	3.56	0	0	0	0.05
66	Mg-OH @ 2.32 $\mu\text{m}$ (serpentine)	Clark et al. (1990)	2	2.22	2.32	2.42	0	0	0	0.05
67	OH @ 1.40 $\mu\text{m}$	Clark et al. (1990)	2	1.3	1.4	1.5	0	0	0	0.05
68	Fe3 @ 0.53 $\mu\text{m}$ (hematite)	This work	1	0.44	0.53	0.614	0	0	0	0.05
69	Fe3 @ 0.624 $\mu\text{m}$ (oxide)	This work	1	0.6	0.624	0.76	0	0	0	0.05
70	Fe3 @ 0.86 $\mu\text{m}$ (oxide)	This work	1	0.755	0.86	0.977	0	0	0	0.05
71	Fe3 @ 0.92 $\mu\text{m}$ (oxide, LCP)	This work	1	0.807	0.92	0.984	0	0	0	0.05
72	Olivine @ 1.08–1.47 $\mu\text{m}$ (weighted sum)	This work	7	0	0	0	0	0	0	0.1
73	H <sub>2</sub> O, OH at 1.395 $\mu\text{m}$	This work	1	1.33	1.395	1.467	0	0	0	0.05
74	H <sub>2</sub> O @ 1.53 $\mu\text{m}$	This work	1	1.367	1.525	1.808	0	0	0	0.05
75	H <sub>2</sub> O @ 1.75 $\mu\text{m}$	This work	1	1.69	1.75	1.815	0	0	0	0.05

Table 1. *Continued.* Parameter descriptions: A list of the 95 spectral indices analyzed in this paper (of the 107 total calculated by Spindex), their source, the equation type, the defining wavelengths and constants, and threshold value. Type corresponds to equation numbers in Fig. S1 in supporting information, and those equations, along with the wavelength positions and constants, allow for the spectral index to be calculated on any spectrum.

#	Parameter	Source	Type	Wavelength positions and constants						Thresh.
76	H <sub>2</sub> O @ 2.13 μm (monohydrated sulfates)	This work	1	1.93	2.132	2.25	0	0	0	0.05
77	Al-OH @ 2.165 μm (pyrophyllite, kaolinite)	This work	1	2.12	2.165	2.23	0	0	0	0.05
78	Al-OH @ 2.185 μm (smectites, poorly crystalline)	This work	1	2.12	2.185	2.25	0	0	0	0.05
79	Si-OH @ 2.160, 2.210 μm (kaolinite)	This work	18	2.12	2.165	2.21	2.235	0	0	0.05
80	Al-OH at 2.21 μm	This work	1	2.165	2.21	2.225	0	0	0	0.05
81	Fe-OH at 2.235 μm (hydroxylated ferric sulfates)	This work	1	2.21	2.235	2.252	0	0	0	0.05
82	Al-OH, Si-OH @ 2.245 μm (opal, other)	This work	1	2.12	2.245	2.34	0	0	0	0.05
83	Si-OH @ 2.210, 2.265 μm (opal)	This work	23	2.165	2.21	2.265	2.35	0	0	0.05
84	Fe-OH, Al-OH @ 2.265 μm (jarosite, gibbsite)	This work	1	2.21	2.265	2.34	0	0	0	0.05
85	Chlorite @ 2.355 μm	This work	1	2.3	2.355	2.45	0	0	0	0.05
86	CO at 2.48 μm (carbonate, Mg-carbonate)	This work	1	2.364	2.48	2.57	0	0	0	0.05
87	CO <sub>2</sub> , H <sub>2</sub> O at 2.6 μm	This work	19	2.456	2.53	2.6	0	0	0	0.05
88	CO @ 3.42 μm (carbonates)	This work	1	3.25	3.42	3.63	0	0	0	0.05
89	CH @ 3.42 μm (organic- aliphatic)	Dartois et al. (2004), Pendleton and Allamanola (2002), Moroz et al. (1998), Merouane et al. (2012), Duley and Williams (1981)	1	3.19	3.415	3.59	0	0	0	0.05
90	DNU—CO <sub>2</sub> @ 4.25 μm	This work	1	4.15	4.25	4.35	0	0	0	0.05
91	Pyroxene @ 0.95, 1.95 μm	This work	11	0.95	1.6	1.95	0	0	0	0.05
101	DNU—NH <sub>4</sub> @ 3.06 μm	Ammannito et al. (2016); De Sanctis et al. (2017)	1	2.9	3.06	3.25	0	0	0	0.05
105	Aromatic CH @ 3.28 μm	This work	1	3.15	3.28	3.7	0	0	0	0.05
106	Fe @ 1.20 μm	This work	13	0.55	1.05	1.596	1.848	2.247	0	1.09
107	CO @ 3.95 μm (carbonate-all)	This work	10	3.63	3.7	3.95	0	0	0	0.07

Our knowledge of both the composition and spectral features of the C chondrites provides our best starting point for the science return from OVIRS measurements of Bennu's surface. As a result, the following minerals and chemicals were specifically targeted for analysis with spectral indices: olivine (forsteritic and fayalitic), pyroxene (orthopyroxene and clinopyroxene), serpentine (Mg, Fe), saponite, mixed layered or poorly crystalline Fe-bearing and clay minerals, magnetite, oxides, hydroxides, carbonates, and organic matter. If these a priori assumptions turn out to be incorrect, then the indices may need to be re-evaluated.

### Parameterizing Spectra for Mission Science

Spectral indices have an established history in planetary science in cases where there is a need to uniformly process and interpret large amounts of spacecraft data (Lucey et al. 1995; Bell et al. 2000; Murchie 2000). The aim is to describe a feature or absorption in the spectrum using a single value, which is defined by algorithmically combining spectral data at certain wavelengths (e.g., Pelkey et al. 2007). The spectral indices (e.g., combination of algorithm and defining wavelengths) for OSIRIS-REx mission science were



compiled from the available literature. A reference for each index can be found in Table 1.

A comprehensive index set was previously created to interpret data from the Compact Reconnaissance Imaging Spectrometer for Mars (CRISM) aboard the Mars Reconnaissance Orbiter (Pelkey et al. 2007; Viviano-Beck et al. 2014), and the resulting mineral maps (“summary products”) have been highly influential for highlighting the diversity and distribution of Martian mineralogy (Wray et al. 2008; Murchie et al. 2009; Thollet et al. 2012). We directly adopted many of the indices from Pelkey et al. (2007) for use at Bennu, but because the expected composition of Bennu differs substantially from that of Mars, we did not incorporate a number of those indices, and we used other sources to ensure inclusive mineral/chemical detection. In total, the OSIRIS-REx team collected 107 spectral indices from the literature for use at Bennu (Table 1). Owing to the diversity of sources from which these spectral indices were collected, the degree to which each index has been proven reliable differs. For instance, some have been tested broadly on Mars spectral data (e.g., Pelkey et al. 2007; Ody et al. 2013), others were developed for asteroid spectra (e.g., Lebofsky 1980; Vilas 1994), and still others were created and tested using (commonly monomineralic) laboratory spectra (e.g., Cloutis et al. 2004, 2006). Whether these indices are applicable outside of the specific scenario for which they were created is an open question, and one this study tests.

Reflectance values are known to represent more than just sample composition. The influence of other factors such as particle size (e.g., Mustard and Hays 1997), albedo (e.g., Clark 1983), space weathering (e.g., Lantz et al. 2015, 2017), temperature (e.g., Bishop and Pieters 1995), and the environment (e.g., vacuum, Takir et al. 2013) on the spectral indices also may be of great consequence. For instance, significant changes in slope of the Bennu spectrum have been attributed to particle size effects (Binzel et al. 2015). Where possible, we tested the sensitivity of spectral indices to each of these factors. However, there are few spectra available that were measured under vacuum. In addition, although space weathering has been studied extensively, its effect on spectra of C chondrites and small bodies such as Bennu is complex (Lantz et al. 2017; Thompson et al. 2019). Therefore, some spectral properties may only be tested and understood with spectral data returned from the mission and ultimately from analysis of the returned sample.

## METHODS

### Spectral Collection

We tested the spectral indices with mineral and meteorite spectra publicly available in the Reflectance

Experiment Laboratory (RELAB), United States Geological Survey Spectral Library version 7 (USGS), and Jet Propulsion Laboratory ECOsystem (JPL) spectral libraries. We also obtained data from the literature and the OSIRIS-REx spectral library (Takir et al. 2013, 2019; Donaldson Hanna et al. 2019). To identify mineral spectra of interest, we performed a keyword search on the entirety of these databases, searching for each of 28 minerals (e.g., olivine minerals: fayalite and forsterite) that are listed in Table 2. We sought meteorite spectra of C chondrites, ordinary (O) chondrites, and ureilites for their high abundances of carbon (as graphite, amorphous carbon, and organic compounds)—a priority for spectral detection with the OSIRIS-REx mission. These meteorites also span a range of aqueous and thermal alteration scenarios and consequently contain the full range of primary silicate and alteration minerals that our spectral indices target.

Candidate test spectra were discarded if they (1) did not show absorptions characteristic of their labeled mineral, (2) appeared to be substantively contaminated by another mineral so that identifying absorptions were obscured, (3) were duplicates or identical repeat measurements of the same sample (e.g., the spliced and unspliced spectra available in RELAB), and/or (4) were physical mixtures or otherwise experimentally altered beyond grinding. Of the original 1340 mineral spectra returned, we found 1149 mineral spectra that met our criteria, and we used them to analyze the spectral indices. We collected an additional 293 meteorite spectra that fit these same criteria as follows: 85 C and O chondrite particulates from RELAB, 60 ureilite particulates from RELAB, 101 C chondrite optically thick slabs (referred to here as chips) from RELAB, 30 C chondrite particulates measured under vacuum (Takir et al. 2013, 2019), and 17 OSIRIS-REx spectral library samples (Donaldson Hanna et al. 2019; Table 2; see Fig. S3 in supporting information for a plot of all meteorite spectra).

For both meteorites and minerals, we collected metadata on the wavelength range, particle size, and sample information for each spectrum if it was available. Because these laboratory spectra have the typical high signal-to-noise ratio of laboratory instruments, we also created a second library of noise-added spectra with 5% random noise added at all wavelengths, which is consistent with the upper limit of noise observed in OVIRS spectra and is within the expected noise for the OVIRS instrument (Reuter et al. 2018). We generated 1000 random noise profiles and added them to each spectrum to determine how noise affects band depths and errors.

## Index Analysis

After collecting our test spectral data set, we calculated 107 spectral indices for every spectrum with Spindex (a portmanteau of spectral index), an IDL-based program that was created by the team for calculating the OSIRIS-REx spectral indices. Spindex was designed to be compatible with OVIRS data that have been photometrically corrected and ratioed to a

perfectly diffuse (Lambert) surface (i.e., reflectance factor), which is equivalent to the reflectance quantity typically measured in a laboratory setting.

We resampled the test spectral data set to the spectral resolution of OVIRS to make it compatible with Spindex. Of the 107 spectral indices, 12 were not included in the analysis; these indices measure slopes or reflectance ratios and will be used to highlight space weathering trends and regional composition at Benu.

Table 2. Mineral, organic, and meteorite spectra: Spectra collected from public databases were from eight mineral/chemical groups representing 23 minerals and five organics. There are 11 groups of meteorite spectra, though most spectra are from C chondrites.

Mineral/chemical group	Mineral/Chemical	# Spectra	Spectral source	
Organics	Alkanes/alkenes	27	27 (U)	
	Benzenes	180	180 (U)	
	Graphitic carbon	17	8 (R), 9 (J)	
	IOM (insoluble organic matter)	15	15 (R)	
	Kerogen	24	24 (Kaplan et al. 2018)	
Carbonates	Calcite	102	65 (R), 8 (U), 29 (J)	
	Dolomite	60	32 (R), 6 (U), 22 (J)	
	Magnesite	55	46 (R), 9 (J)	
Olivines	Fayalite (Fo < 50)	33	19 (R), 8 (U) 6 (J)	
	Forsterite (Fo > 50)	30	29 (R), 1 (U)	
Pyroxenes	Augite	36	34 (R), 2 (U)	
	Enstatite	70	38 (R), 26 (U), 6 (J)	
	Ferrosilite	3	3 (R)	
	Hedenbergite	5	5 (R)	
	Pigeonite	21	16 (R), 5 (U)	
Oxides	Chromite	23	13 (R), 2 (U), 8 (J)	
	Hercynite	5	5 (R)	
	Ilmenite	36	32 (R), 4 (U)	
	Magnetite	47	32 (R), 10 (U), 6 (J)	
	Antigorite	20	5 (R), 14 (U), 1 (J)	
Serpentines	Chrysotile	10	7 (R), 2 (U), 1 (J)	
	Cronstedtite	4	3 (R), 1 (U)	
	Lizardite	10	2 (R), 7 (U), 1 (J)	
	Montmorillonite	110	78 (R), 23 (U), 9 (J)	
Smectites	Nontronite	94	72 (R), 9 (U), 13 (J)	
	Saponite	20	14 (R), 3 (U), 3 (J)	
Other	Chlorite	92	6 (R), 50 (U), 6 (J)	
Total: 1149				
Meteorite class	Meteorite group	# Spectra	Spectral source	
C chondrites	CI	7	4 (R), 3 (Takir et al. 2013, 2019)	
	CM	124	108 (R), 16 (Takir et al. 2013, 2019)	
	C-ungrouped	40	37 (R), 4 (Takir et al. 2013, 2019)	
	CR	10	7 (R), 3 (Takir et al. 2013, 2019)	
	CH	4	3 (R), 1 (Takir et al. 2013, 2019)	
	CV	15	11 (R), 4 (Takir et al. 2013, 2019)	
	CO	14	14 (R)	
	CK	4	4 (R)	
	Ordinary chondrites	L	5	5 (R)
	Ureilites	Ureilites	60	60 (R)
	Other	Analog mixture	10	10 (OSIRIS-REx Spectral Library)
Total: 293				

R = RELAB Spectral Library, U = USGS Spectral Library, J = JPL ECOSystem Spectral Library.

For the remaining 95 indices, Spindex uses 21 different equation types that range from a typical band depth measurement (Clark and Roush 1984) to more complex weighted sums that take into account reflectance values at up to five or more different wavelengths (i.e., Ody et al. 2012; see Fig. S1). Table 1 contains a full list of these indices, a reference to the equation used to calculate them, the defining wavelengths, and a threshold value. The threshold is an estimate of the minimum valid band depth value for the index, which is defined by OVIRS instrument noise requirements (Reuter et al. 2018; Simon et al. 2018).

Spindex produces a number of data products in relation to each spectrum, including band depths, errors on those band depths, band presence (e.g., whether band depth is above or below the designated threshold), and reflectance at 0.5  $\mu\text{m}$ . Although the threshold was an integral part of this analysis, Spindex reports band depth values regardless whether they fall above the threshold, and we include this information where possible. In addition, we compared the calculated band depths with mineralogy (for the meteorite spectra), particle size, and reflectance at 0.55  $\mu\text{m}$  to determine (1) the relationship between index value and composition, if any and (2) the influence of non-compositional variables most likely to affect band depth.

An uncertainty value (band sigma) is computed for every spectral index. We use the root mean square (rms) of the spectral values in a  $\pm 16$  nm wavelength interval for each wavelength that defines the band parameter as the adopted uncertainty. In OVIRS spectra shortward of 2.4  $\mu\text{m}$ , the spectral resolution is resampled to 2.0 nm, so the 32 nm range (16 nm in each direction) includes 15 or 16 channels. The uncertainties in the calibrated spectra due to read noise, thermal noise, gain, and other instrumental sources, along with the absolute calibration and photometric correction, are also included and added to the rms noise in quadrature. For each band calculation, these uncertainties in the input band center and continuum values are propagated according to the band depth formula using a Taylor expansion (Bevington 1969).

To test index performance, we visually evaluated every spectrum along with its Spindex output and determined whether the Spindex-identified absorption features were positive, negative, false positive, or false negative. A positive was recorded if the spectral index identified a spectral feature as being present (i.e., above threshold), and the feature was in fact present. Likewise, a negative result was recorded if the spectral index did not identify the spectral feature, and the feature was not present. A false positive result was recorded if the spectral index identified the spectral feature, but the feature was not present. Finally, a false negative was

recorded when the spectral index did not identify a feature, but that feature was present. However, owing to the difficulty of correctly determining the mineral/chemical source of the absorption and estimating whether the absorption was stronger than the threshold, false negatives were likely underreported. Because of the high likelihood of inconsistencies, we do not report the false negative results (although they were helpful in determining updates needed for Spindex—i.e., new indices or index adjustments). Thus, indices with high rates of positives and negatives and low rates of false positives were designated as reliable indices.

## RESULTS

### Minerals

We tested the indices on 1149 spectra of 28 different minerals/organics (Table 2) to determine how the indices perform in the most ideal case, where each spectrum represents a single, pure phase. These tests allowed us to identify indices that have a high rate of positive identification for the phase of interest and return a low rate of false positives for other minerals/organics. We discuss a few examples along with a summary of the overall findings, and all results are presented in Tables S1.1–S1.13 in supporting information.

In the first example, we tested a spectral index targeting pyroxene (#47: pyroxene at 1.9  $\mu\text{m}$ ) on spectra of the pyroxene minerals augite, hedenbergite, pigeonite, ferrosilite, and enstatite (Figs. 1a and 1c). Using this index, 83% of the pyroxene spectra have band depths stronger than 5%, so a majority of the pyroxenes are positively identified. If we break these results down by pyroxene mineral, however, the Ca-rich clinopyroxenes (hedenbergite, augite, and pigeonite) typically exhibit weaker band depths, whereas enstatites and ferrosilites almost always exceed the 5% band depth threshold (Fig. 1a). When we compare the spectra of the pyroxenes, this discrepancy appears to be due to the longer-wavelength position of the Ca-rich clinopyroxene 2  $\mu\text{m}$  band, which is not well captured by the wavelengths defining this index (Fig. 1c). Ideally, we want indices that positively identify pyroxene any time it is present in a spectrum, in addition to indices that can be used to distinguish between low-calcium and high-calcium pyroxenes.

We are equally interested in how a spectral index deals with spectra of minerals that are not targeted by that index. For example, when the pyroxene index above is tested on all 1149 mineral spectra, it returns a false positive 18% of the time (i.e., positively detects pyroxene where a visual inspection reveals no pyroxene). An example of the positive, negative, and false positive results for six different



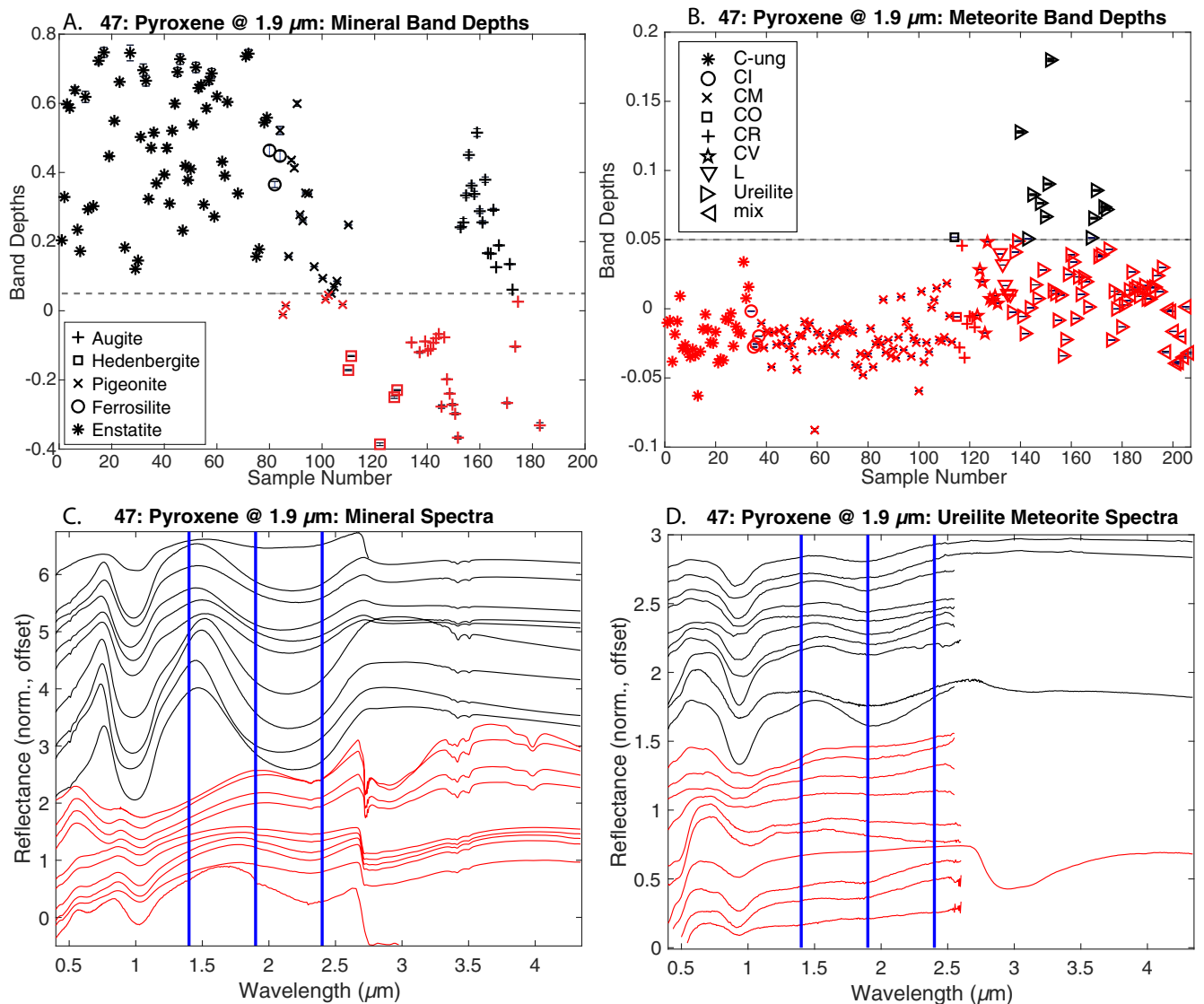


Fig. 1. Spindex results for a pyroxene parameter. A, B) Band depths calculated with parameter #47, pyroxene at 1.9  $\mu\text{m}$ , are plotted for pyroxene mineral spectra (A) and meteorite spectra (B). Black designates a band depth above the threshold, and red is below. Symbols are used to differentiate pyroxene minerals and meteorite groups. The threshold value for this parameter is shown as a dashed line. C, D) A subset of the spectra from which each of these band depths was calculated; the spectra are normalized at 0.55  $\mu\text{m}$  and offset so that the top 10 spectra (black) and bottom 10 (red) correspond to band depth values above and below the threshold. C-ung, ungrouped C chondrite. All meteorite spectra in this study can be viewed individually in Fig. S3. (Color figure can be viewed at [wileyonlinelibrary.com](http://wileyonlinelibrary.com).)

indices shown in Fig. 2, with the results tabulated by mineral. In some cases where there are overlapping absorption features (e.g., pyroxene and olivine at 1  $\mu\text{m}$ ) we expect a higher rate of false positives, so results broken down by mineral allow for a fuller assessment of index performance (Fig. 2, Tables S1.1–S1.13).

These tests demonstrate that most indices work as expected for pure mineral spectra. For instance, an olivine index defined in Pelkey et al. (2007; #48: olivine at 1.05–1.47  $\mu\text{m}$ ) positively identifies the 1- $\mu\text{m}$  feature in both fayalitic (forsterite number, Fo, <50) and forsteritic

(Fo >50) olivine (Fig. 2a). However, this index also generates false positives for a number of the other minerals, usually as a result of a non-olivine iron absorption near 1  $\mu\text{m}$ . In another example, a serpentine index (#66: Mg-OH at 2.32  $\mu\text{m}$ ) also performs well for the targeted serpentine minerals (antigorite, chrysotile, cronstedtite, and lizardite), but likewise returns many false positives for carbonates, organics, and clays due to their absorption features in the 2.2–2.5  $\mu\text{m}$  region (Fig. 2b). Indices #89 and #107—targeting aliphatic organics at 3.42  $\mu\text{m}$  and carbonate at 3.95  $\mu\text{m}$ ,

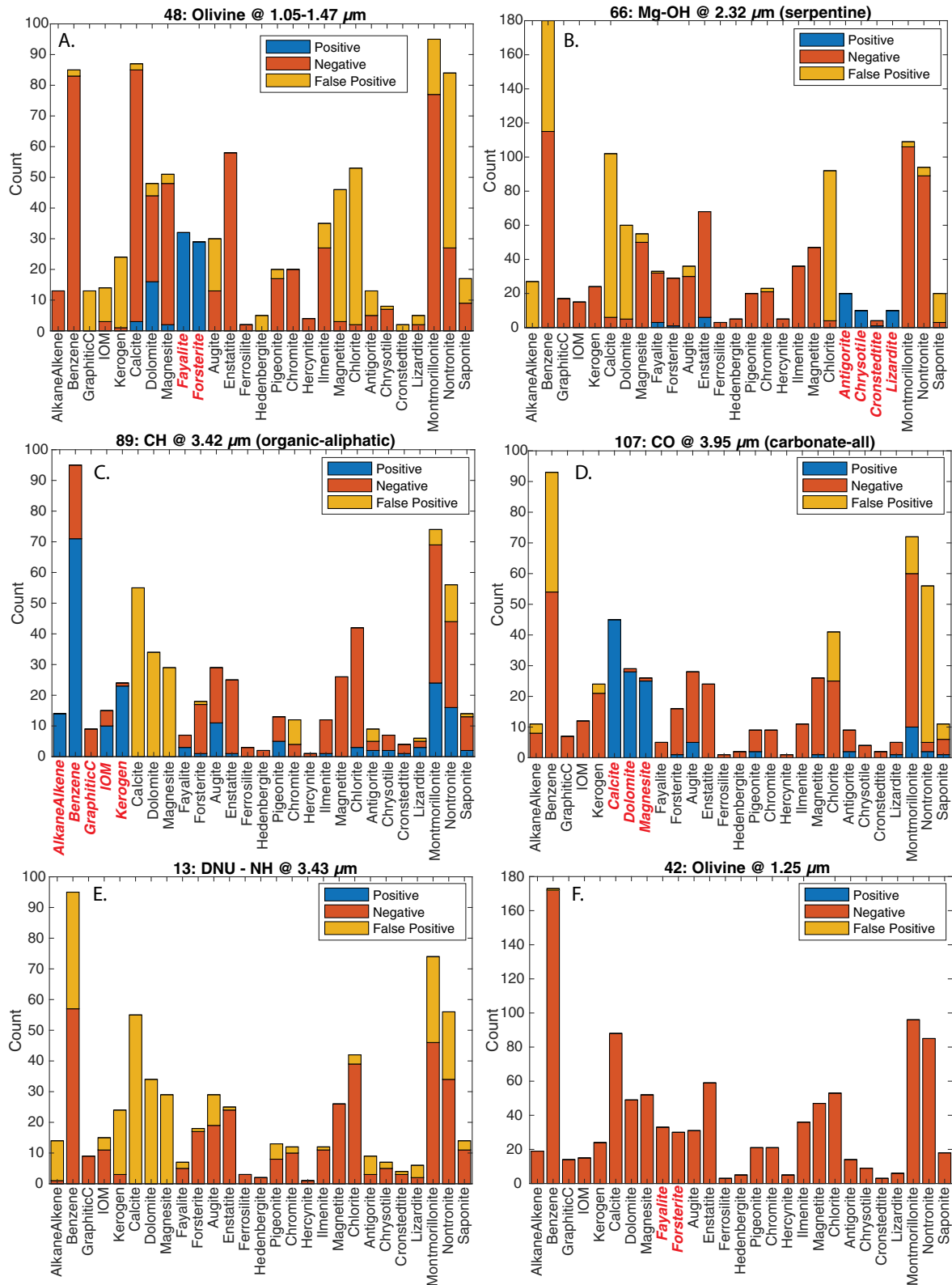


Fig. 2. Positive, negative, and false positive results for minerals. A–F) The number of times each of six spectral parameters returned a positive, negative, or false positive result is tabulated. The results are broken down by mineral, with the minerals that the parameter targets italicized in red (e.g., parameter #48 targets the olivine minerals forsterite and fayalite). More information on the minerals and the number of spectra in each can be found in Table 2. (Color figure can be viewed at [wileyonlinelibrary.com](http://wileyonlinelibrary.com).)

respectively—are two examples that perform well (>75% positive detections) for their target mineral/chemical and have false positives concentrated in specific minerals (Figs. 2c and 2d). The aliphatic organics absorption at 3.4  $\mu\text{m}$  overlaps with a carbonate absorption at that same wavelength, so this index returns false positives specifically for the carbonate minerals calcite, dolomite, and magnesite. Aliphatic organics are also found as contaminants in many of the pure minerals, accounting for the higher rate of positive detections of index #89 for all minerals/chemicals.

In a small number of cases, indices perform poorly even on their target minerals. Figures 2e and 2f shows two extreme examples: indices #13 (NH at 3.43  $\mu\text{m}$ ) and #42 (olivine at 1.25  $\mu\text{m}$ ). Indices that return only false positives, without any positive results, are concerning owing to the likelihood of misinterpretation when mapping Bennu and have been labeled “Do Not Use (DNU).” Most of these indices target absorption features that overlap with the strong OH/H<sub>2</sub>O absorption at 3  $\mu\text{m}$ . These indices are likely to be useful for many applications, but may be unsuitable for application to Bennu given the presence of a global 3- $\mu\text{m}$  absorption band (Hamilton et al. 2019).

## Organics

Organics are one of the highest-priority materials targeted by OVIRS observations because the primary mission objective is to return volatile- and organic-rich material from the early solar system. Absorptions due to aromatic CH at 3.28  $\mu\text{m}$  (#105) and aliphatic CH at 3.42  $\mu\text{m}$  (#89) were chosen as the most likely features to be seen on Bennu based on the C chondrites (e.g., Schmitt-Kopplin et al. 2010; Kebukawa et al. 2011; Orthous-Daunay et al. 2013; Alexander et al. 2017). This expectation is consistent with previous remote detections (e.g., Pendleton and Allamandola 2002; Dartois et al. 2004; Campins et al. 2010; Rivkin and Emery 2010; Cataldo et al. 2013; Chiar et al. 2013). Previous work has shown that band depth at 3.42  $\mu\text{m}$  is strongly correlated with the hydrogen to carbon ratio (H/C) in pure, insoluble organics extracted from meteorites and sedimentary rocks (Kaplan and Milliken 2018; Kaplan et al. 2019). Because insoluble organic matter (IOM) constitutes the majority of the organic matter in C chondrites (Alexander et al. 2017), we used IOM spectra as the most reliable test of the organic spectral indices. We find that the IOM with the highest H/C values has aliphatic absorption features (#89) greater than the 5% threshold, but there are no aromatic absorptions greater than 5%.

In laboratory spectra of meteorites, the aliphatic organic absorption is rarely detected at >5% band depths, and aromatic absorptions are not observed

(Kaplan et al. 2019). However, if we change the threshold for detection of the aliphatic absorption to 4%, we find that there are 30% more positive organic detections in the meteorites and still <4% false positives (i.e., these are real detections in the meteorite spectra). If the threshold is 3%, there are nearly double the positive organic detections for the meteorite spectra, and the false positive detection rate increases to 8%. The original 5% threshold is defined by expected OVIRS performance during the mission, but it may be necessary to lower the threshold of valid band depths for this index to detect organics on Bennu. Tests on the meteorite spectra show that this can be done without greatly increasing the number of false positive detections.

## Meteorites

The meteorite test spectra help establish how well the indices work on heterogeneous materials that are our current closest approximation to Bennu’s surface. The C chondrite spectra have lower overall reflectance and fewer absorption features (particularly features with >5% depth) than the pure mineral spectra. Prominent features in the meteorite spectra include Fe-related absorptions from 0.5 to 1.2  $\mu\text{m}$  and the OH/H<sub>2</sub>O absorptions from 2.7 to 3  $\mu\text{m}$  (Cloutis et al. 2011a, 2011b). Many of the C chondrites also have spectral features associated with organics and carbonate (3.4 and 4  $\mu\text{m}$ ). Although some C chondrites have weak pyroxene and olivine absorption features (1 and 2  $\mu\text{m}$ ), only the ureilites—rare stony meteorites with high carbon content (e.g., Berkley et al. 1980)—routinely have olivine and pyroxene absorptions with >5% band depths (Figs. 1b and 1d).

Indices tested on the C chondrite spectra produce weaker band depths, resulting in fewer positive detections and fewer false positive detections than for the mineral spectra. This trend is likely due to the presence of opaques that reduce the overall reflectance and band depths of these samples. Indices applied to the meteorite spectra have, on average, ~2% false positives, compared with the 9% average false positive returns for the pure mineral spectra. Only half of the 95 indices are ever observed above their threshold value and, of these positive detections, more than 80% are due to the four indices that measure the 3- $\mu\text{m}$  region.

Absorptions associated with hydrated minerals at 0.7 and 2.7–3  $\mu\text{m}$  are of particular interest for the OSIRIS-REx mission because Bennu is thought to be a fragment of a larger asteroid that experienced intense hydrothermal alteration early in solar system history (Lauretta et al. 2015). Index #7, targeting OH at 2.7  $\mu\text{m}$ , results in band depths surpassing the 5%

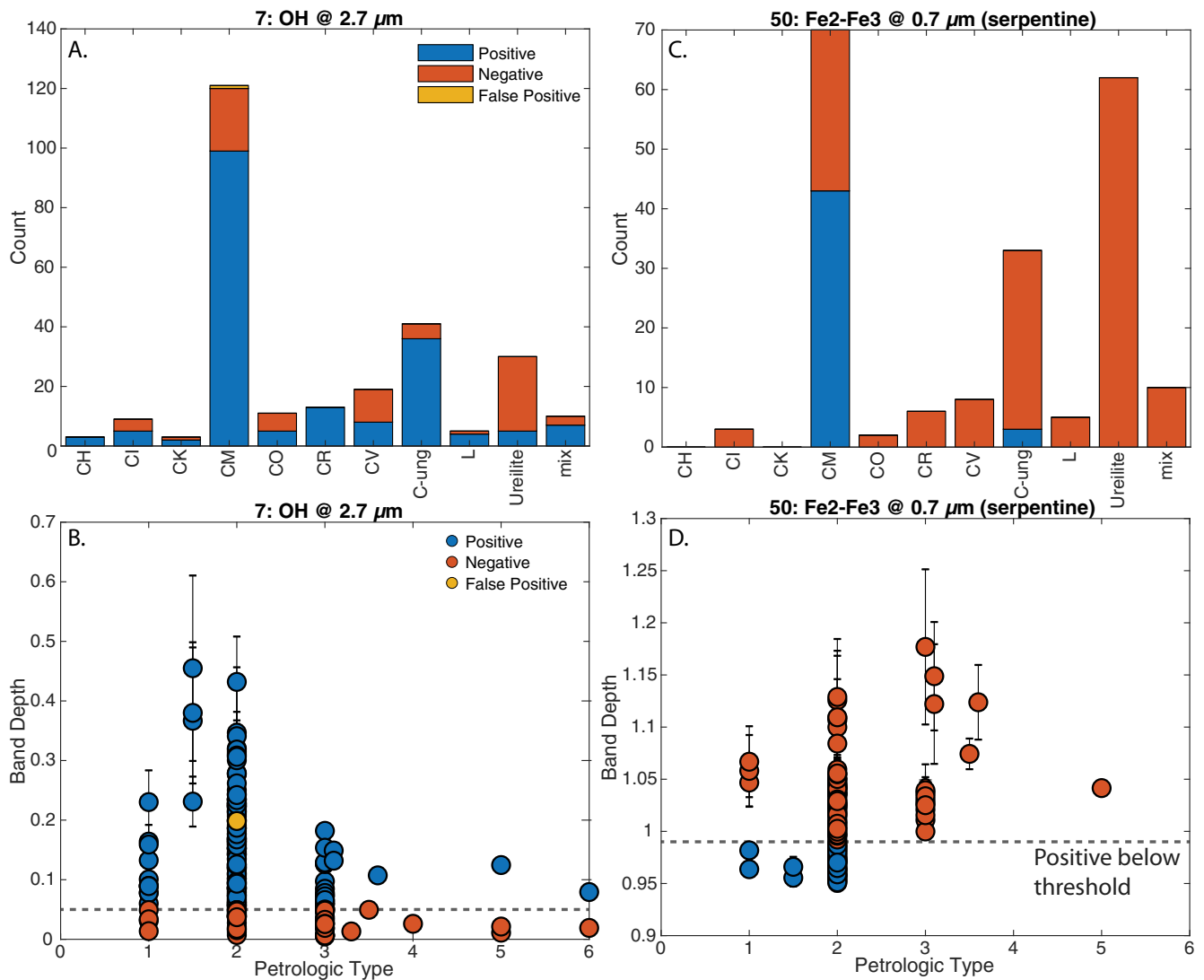


Fig. 3. Positive, negative, and false positive results for meteorites. A, C) Positive, negative, and false positive results are tabulated for two spectral parameters (#7: OH @ 2.7  $\mu\text{m}$ , a; #50: Fe2-Fe3 @ 0.7  $\mu\text{m}$  in serpentine, C) broken down by meteorite classification group. B, D) Band depth for each parameter compared with petrologic type of the meteorites. Count refers to the number of spectra, where each bar sums to the total number of spectra for that meteorite group. (Color figure can be viewed at [wileyonlinelibrary.com](http://wileyonlinelibrary.com).)

threshold in 62% of meteorite spectra. This absorption feature is least prominent in the pristine ureilites and most prominent in aqueously altered CI, CR, and CM chondrites (Fig. 3a). In fact, the band depth of this 2.7- $\mu\text{m}$  absorption becomes weaker with increasing petrologic type (i.e., Beck et al. 2014; Garenne et al. 2016), which corresponds to decreasing aqueous alteration and increasing thermal processing (Fig. 3b). Other indices associated with the 3  $\mu\text{m}$  region (#3, #4, and #52) showed comparable results, but may be more strongly influenced by adsorbed terrestrial water in spectra measured under ambient conditions. The 0.7  $\mu\text{m}$  band is positively identified in fewer meteorite spectra (15%) and is even more specifically associated with

spectra of aqueously altered C chondrites, as it is only observed in the CM and C-ungrouped meteorites (Figs. 3c and 3d). All of the meteorites with a 0.7  $\mu\text{m}$  absorption are petrologic type 1 or 2, the most aqueously altered of the meteorites.

A small portion of the meteorite spectra used in this study (30 of 293 total spectra) were measured under vacuum, and all of these are of C chondrites. Takir et al. (2013) demonstrated that the vacuum environment reduces the strength of the 3  $\mu\text{m}$  H<sub>2</sub>O absorption in these spectra by removing adsorbed terrestrial water. However, even with the adsorbed water absent, we detect a 3  $\mu\text{m}$  absorption (#3, H<sub>2</sub>O/OH at 3  $\mu\text{m}$ ) in 78% of these vacuum spectra. By comparison, this

Table 3. Best parameters: A list of the 17 parameters that are most likely to be useful for detecting absorption features in spectra of carbonaceous chondrites. Rates of detection (positive %) and false positive returns (false positive %) are reported for the meteorite and mineral test; breakdown of these numbers by meteorite group or mineral is found in Tables S1.1–S1.13. Notes describe where parameters performed similar to others or were included for a specific reason.

#	Parameter name	Target	% Pos mineral	% False pos mineral	% Pos meteorite	%False pos meteorite	Notes
46	Pyroxene @ 1.05 $\mu\text{m}$ (wide)	Pyroxene—general	89.92	13.68	13.00	5.67	Performs similarly to #91
47	Pyroxene @ 1.9 $\mu\text{m}$	Pyroxene—general	83.75	18.43	4.67	0.00	
71	Fe3 @ 0.92 $\mu\text{m}$ (oxide,LCP)	Pyroxene—LCP versus HCP	83.77	0.49	4.67	0.00	
43	Olivine @ 1.01–1.36 $\mu\text{m}$ (Lo-Fe)	Olivine—general	98.28	18.27	4.67	13.33	High false positive due to overlap with pyroxene/other
48	Olivine @ 1.05–1.47 $\mu\text{m}$	Olivine—general	100.00	23.52	6.00	21.00	High false positive due to overlap with pyroxene/other
107	CO @ 3.95 $\mu\text{m}$ (carbonate-all)	Carbonate—general	98.45	10.50	2.33	0.33	
38	CO @ 3.95 $\mu\text{m}$ (carbonate-calcite)	Carbonate—Ca versus Mg	69.76	8.31	1.67	0.00	Detects calcite (100% positive) over dolomite (34% positive) and magnesite (23% positive)
7	OH @ 2.7 $\mu\text{m}$	Phyllosilicates—general	86.11	2.22	62.33	0.33	
52	OH,H <sub>2</sub> O @ 2.85 $\mu\text{m}$	Phyllosilicates—general	99.96	6.22	76.67	2.33	
3	H <sub>2</sub> O,OH @ 3 $\mu\text{m}$	Phyllosilicates—general	99.51	1.19	80.67	0.67	Performs similarly to #4
6	H <sub>2</sub> O,OH @ 1.93 $\mu\text{m}$	Phyllosilicates—general	72.39	5.37	0.67	0.00	
66	Mg-OH @ 2.32 $\mu\text{m}$ (serpentine)	Phyllosilicates—specific	100.00	31.01	1.00	0.33	
50	Fe2-Fe3 @ 0.7 $\mu\text{m}$ (serpentine)	Ferrous minerals	19.97	5.20	15.33	0.00	
70	Fe3 @ 0.86 $\mu\text{m}$ (oxide)	Ferric minerals	5.57	2.97	2.33	3.00	Detects band near 0.9 $\mu\text{m}$ in meteorites; high false positive due to overlap with olivine/pyroxene
89	CH @ 3.42 $\mu\text{m}$ (organic-aliphatic)	Organics—aliphatic	79.59	12.31	3.67	0.67	Thoroughly tested on insoluble organics (Kaplan et al. 2018)
105	Aromatic CH @ 3.28 $\mu\text{m}$	Organics—aromatic	59.86	11.24	0.00	0.00	Detected with Rosetta (Capaccioni et al. 2015); ~1% feature in some meteorite spectra

absorption is detected in 99% of the C chondrite particulates measured under ambient conditions and in 94% of the C chondrite chip spectra, which are also measured under ambient conditions but are expected to be less affected by adsorbed water than the particulates (Fig. S2 in supporting information). Given the predominance of ambient spectra in our collection, the positive detection rates and band depths at 3  $\mu\text{m}$  are overestimates, although the vacuum spectra confirm that this feature is still likely to be observed with our indices for asteroids and other space observations.

### Summary of Mineral, Organic, and Meteorite Tests

We identified the 17 indices that are most likely to perform well for carbonaceous meteorites, the surface of Bennu, and similar asteroid surfaces (Table 3). This selection was guided by the expected mineralogy/chemistry of bodies such as Bennu as described earlier (i.e., minerals/chemicals we want to be able to detect), and the results of the index tests (i.e., how good we are at detecting them), with the results of the meteorite analysis prioritized over the pure mineral/chemical



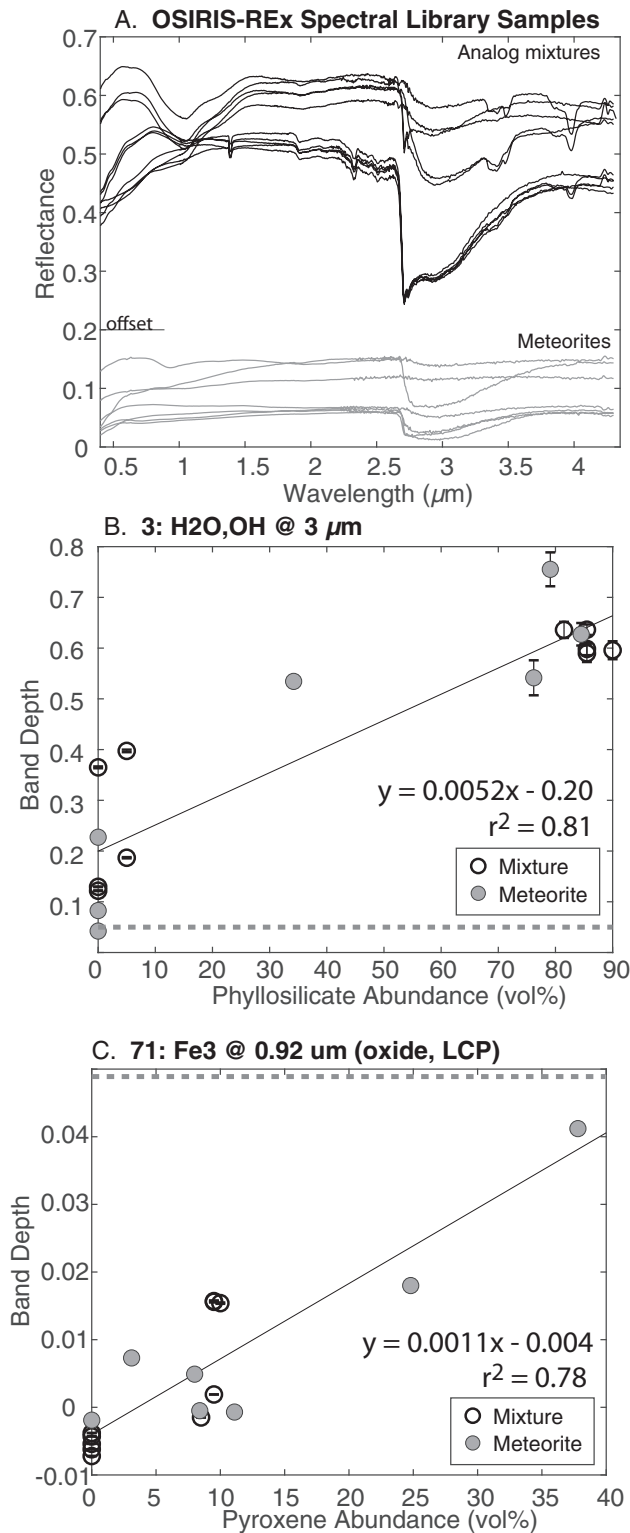


Fig. 4. OSIRIS-REx spectral library composition. A) The OSIRIS-REx spectral library meteorite and meteorite analog spectra, offset to distinguish the meteorites (gray) and analog mixtures (black). B, C) Relationship between band depth and mineral abundance (vol.%) for phyllosilicates (B) and pyroxene (C). The threshold is shown as a dashed line.

results (Tables S1.13 and S1.1–S1.12, respectively). This subset of indices targets olivines, pyroxenes, phyllosilicates, ferrous minerals, carbonates, and organics. Most of these indices yield positive detections in >80% of cases for the pure minerals. Those that result in a lower fraction of successful cases were chosen specifically because they worked well for meteorites or filled a needed niche (e.g., aromatic organics).

## COMPOSITION, ALBEDO, PARTICLE SIZE, AND SIMULATED INSTRUMENT NOISE

### Composition

We collected 17 well-characterized meteorite and analog mineral mixture spectra as part of preparation for the OSIRIS-REx spectral measurements with OVIRS and the OSIRIS-REx Thermal Emission Spectrometer (OTES; Christensen et al. 2018). This library consists of particulate samples measured under ambient conditions at the OVIRS and OTES wavelengths without added noise. Donaldson Hanna et al. (2019) reported the team's spectral interpretation of the samples, focusing on the OTES wavelengths. We compared mineral abundances and band depths for the OSIRIS-REx spectral library samples to understand the relationship, if any, between index strength and composition (Fig. 4). We collected the meteorite mineral abundances from literature (Howard et al. 2015) and measured them directly (Donaldson Hanna et al. 2019), but the meteorites are known to be heterogeneous, so we cannot be certain that the sample aliquots measured spectrally are identical in mineralogy to those in the literature or even the thin sections of our own samples.

We find multiple indices that are correlated with mineral abundance. Fit using a linear regression, the relationships reported here have  $r^2 > 0.6$ , and in some cases as high as 0.82. First, pyroxene abundance is correlated with three indices (#25, #56, and #71) that measure band depth near 0.9  $\mu\text{m}$ . However, the pyroxene band depths are all below the 5% detection threshold. Given how weak many of the meteorite absorption features are, it may be important to map and assess band depths below the 5% instrument threshold at Bennu. Phyllosilicate abundance is correlated with indices (#3, #4, #7, and #52) that measure the 3- $\mu\text{m}$  feature between 2.7  $\mu\text{m}$  (OH) and 3  $\mu\text{m}$  (OH/H<sub>2</sub>O) (Fig. 4). The 3- $\mu\text{m}$  absorption band depths are greater than the 5% threshold, although the strength of this feature may be artificially increased by the presence of adsorbed terrestrial water (Takir et al. 2013), which likely explains why some samples with 0 vol% phyllosilicates have band depths that exceed zero. Garenne et al. (2016) demonstrated a linear relationship between 2.8- $\mu\text{m}$  band depth and H wt% for C chondrite spectra measured under vacuum ( $r^2 = 0.66$ ),

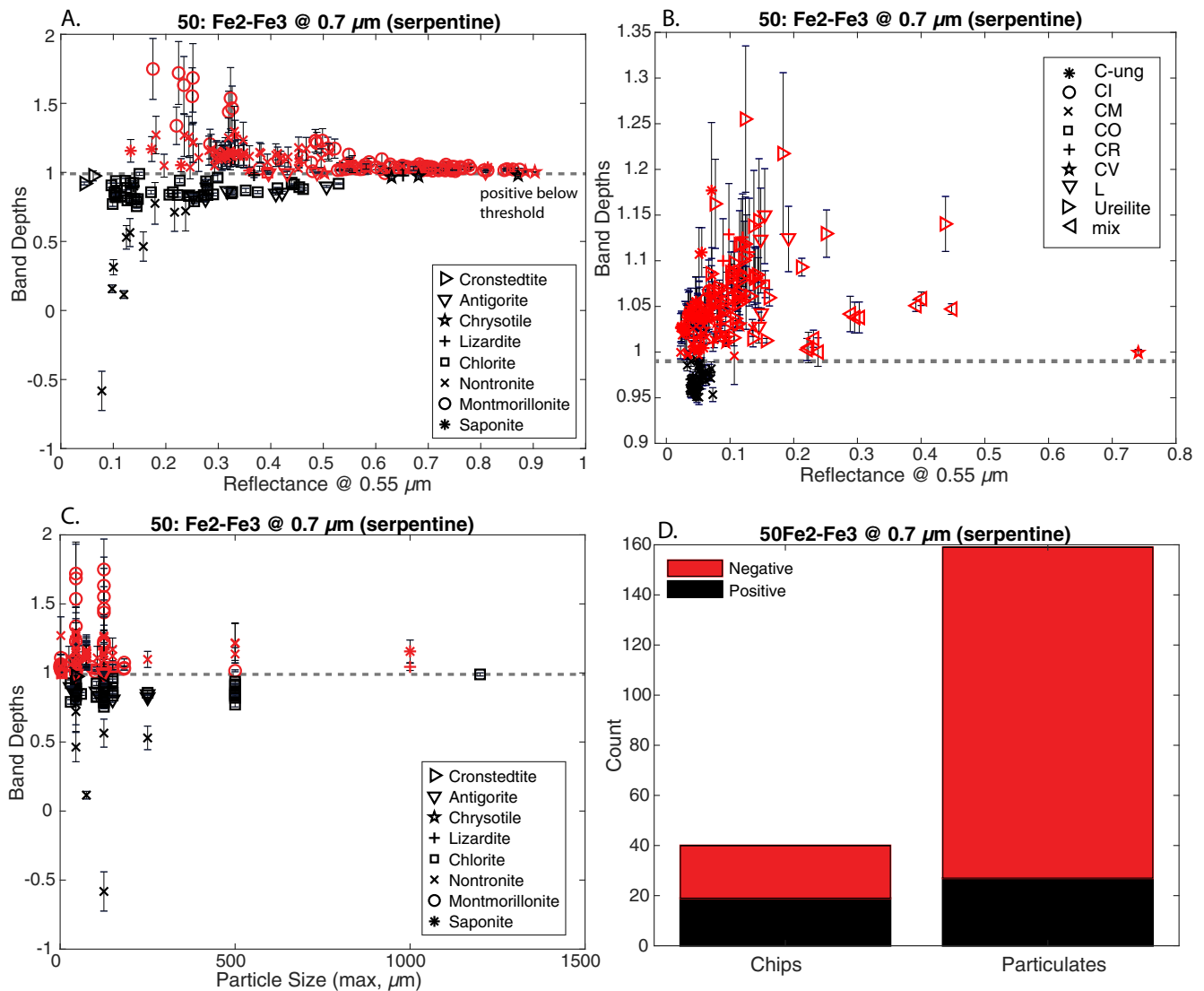


Fig. 5. Particle size and albedo versus band depths. A, B) Band depth for parameter #50 (Fe<sub>2</sub>-Fe<sub>3</sub> @ 0.7 μm—serpentine) is plotted against reflectance at 0.5 μm for hydrated minerals (A) and meteorites (B). For this parameter, band depths below the threshold of 0.99 are positive detections (black), and those above the threshold are negative detections (red); the threshold is shown as a dashed line. C) Band depth versus maximum particle size for the hydrated minerals and (D) the numbers of chip and particulate meteorites with (positive, black) and without (negative, red) a 0.7 μm absorption feature. (Color figure can be viewed at [wileyonlinelibrary.com](http://wileyonlinelibrary.com).)

where H wt% is a proxy for phyllosilicate abundance, suggesting that a relationship exists regardless of whether adsorbed water is present. Ultimately, coordinated spectral and compositional measurements (e.g. X-ray diffraction, microprobe) for a larger number of samples are needed to provide further evidence for band depth–compositional relationships in meteorites.

### Albedo and Particle Size

Because the spectra collected for this study were measured for many purposes, the variable measurement conditions allow us to test the effects of sample and

spectral properties on the Spindex indices. In particular, it is important to know how these indices respond to spectra of natural surfaces with variable particle size and albedo. For most minerals and the meteorites, we have enough spectra (Table 2) that a wide range of albedos is represented by the data set (e.g., see Fig. 5 for range of reflectance at 0.55 μm for serpentines and meteorites). In addition, the data set includes spectra of both chips and particulates; particulate size fractions range from <10 to >1000 μm, with <45 μm being the most common particle size.

We compared the reflectance at 0.55 μm with band depth for each of the indices and found no correlations.

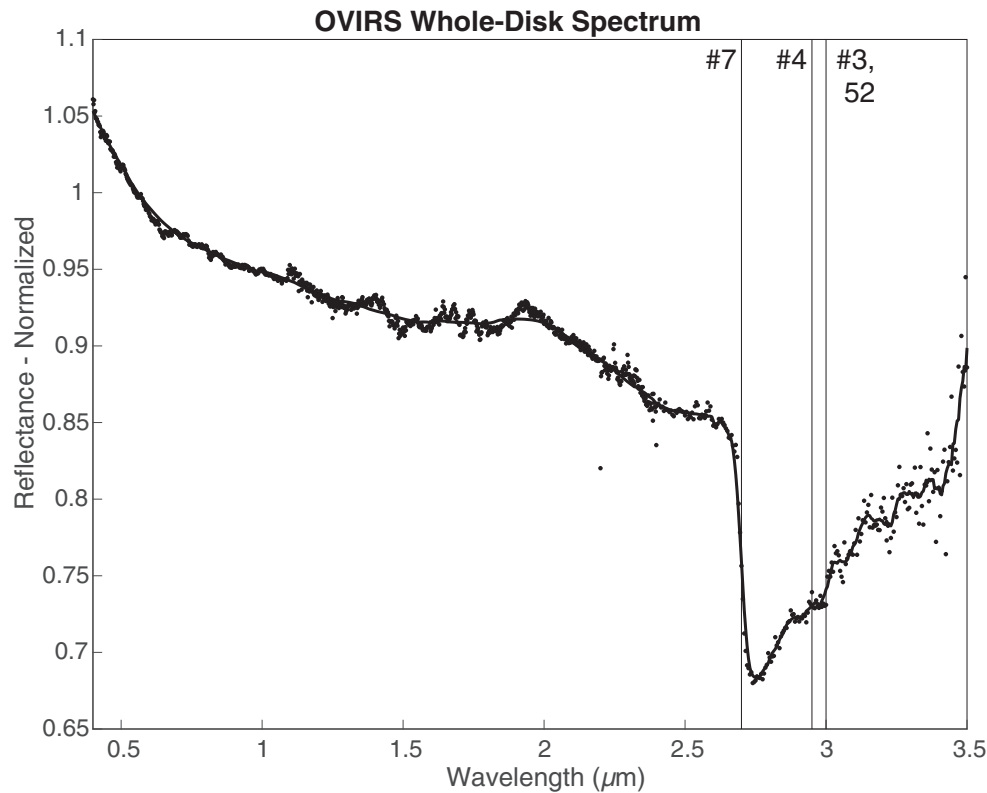


Fig. 6. Bennu Spectrum: An average radiance factor spectrum of asteroid Bennu collected by the OVIRS instrument, normalized at 0.55  $\mu\text{m}$ . The center position of the four 2.7–3  $\mu\text{m}$  spectral indices are indicated with a labeled vertical line. The OVIRS data were acquired on November 2, 2018 when the OVIRS field of view was approximately 40% filled.

Reflectance at 0.55  $\mu\text{m}$  was used because it corresponds to the V passband (e.g., filter centered at 0.55  $\mu\text{m}$  used in broad-band photometry) and is the most common wavelength for reporting geometric albedo or normal reflectance of asteroids. Band depths weaken as albedo decreases (Nash and Conel 1974; Clark 1983; Milliken and Mustard 2007), so if an albedo effect is present, we would expect to see a positive correlation between reflectance at 0.55  $\mu\text{m}$  and the band depth returned by each index. Figures 5a and 5b shows one such comparison for index #50 ( $\text{Fe}^{2+}$ - $\text{Fe}^{3+}$  at 0.7  $\mu\text{m}$  in serpentine) for both serpentine mineral spectra and meteorite spectra. In this case, the index appears to have the strongest band depth at the lowest reflectance values. This association between albedo and band depth is likely a result of this absorption feature arising in only the most aqueously altered C chondrites, which are also the lowest-albedo samples.

As with albedo, we observe no particle size effect in these data. In VIS-NIR spectra, samples with the smallest (<10  $\mu\text{m}$ ) and largest (>500  $\mu\text{m}$ ) particle sizes have the weakest band depths because of the dominance of surface scattering and absorption, respectively, over volume

scattering (e.g., Hapke 1993; McGuire and Hapke 1995; Mustard and Hays 1997). Laboratory spectra are commonly measured on powders ground to an intermediate particle size of <45  $\mu\text{m}$  to maximize volume scattering. We analyzed the meteorite spectra with a 0.7  $\mu\text{m}$  absorption and found that this absorption is observed at all particle sizes, including for chips. There are as many detections as non-detections (above and below threshold) at all particle sizes for this spectral index (Figs. 5c and 5d). The mean, mode, or distribution of particle sizes in the samples is rarely reported, so it is possible that the maximum particle size, which is used here, does not accurately represent effective sample particle size. The meteorite spectra fall into two distinct particle sizes, chips and particulates, where chips are expected to have weaker absorptions features (Kaplan et al. 2019). Interestingly, within the meteorite spectra, a greater proportion of the chips have a 0.7  $\mu\text{m}$  feature than the particulates. Again, this difference is likely a result of compositional variability between the two groups rather than a particle size effect; the chip samples are primarily CM-group C chondrites, which are likely to have a 0.7  $\mu\text{m}$  absorption, whereas the particulate samples also includes ureilites, ordinary

chondrites, and thermally processed C chondrites that typically do not have this absorption feature. All other indices also lack a relationship with particle size.

### Noise

We see small systematic differences in Spindex results when  $\pm 5\%$  random noise is added to every spectrum. This degree of noise is chosen as a worst case scenario for OVIRS assuming the noise needs to be  $< \pm 4.4\%$  to detect a 5% absorption feature on a 3.5% reflectance body (Reuter et al. 2018; Simon et al. 2018). Spindex calculations account for noisy data by averaging six or more channels for every wavelength calculation; thus small, single-channel spikes should not disproportionately affect the calculation. There is a possibility of removing real absorption features or adding spurious ones when noise is present. However, we find that 5% noise does not strongly affect the interpretation of absorption features in the spectrum. For instance, our original, noise-free spectrum of the Murchison meteorite does not have a 3.42  $\mu\text{m}$  organic absorption feature and, appropriately, when index #89 (CH at 3.42  $\mu\text{m}$ —aliphatic organics) is calculated on that spectrum, band depth is close to zero. When this index is calculated on 1000 Murchison spectra with added noise, the 3.42  $\mu\text{m}$  band depth varies from  $-0.062$  to  $0.027$ . None of the noise-added spectra have band depths greater than the 5% threshold. We find similar results for the index #7 (OH at 2.7  $\mu\text{m}$ ), which was originally above the threshold value, and noise-added spectra all have a band depth  $> 5\%$ .

Band depth is highly correlated with the error value on that band depth (e.g.,  $r^2 = 0.96$  for index #89 calculated on Murchison), in such a way that error is minimized when band depth is closest to the true (noise-free) band depth. The largest, spurious band depths also have the largest errors, which means they are more likely to be identified and removed during spectral analysis and mapping.

### CAVEATS

Spectral indices are a useful method for collapsing hyperspectral data into a single data point, which enables rapid assessment of spectra and provides a straightforward value for mapping, but there are important caveats to consider when using index values instead of full spectra. The first is that abundance and band depth are not necessarily correlated. Although a small number of indices appear to have band depths that increase with mineral abundance (Figs. 4b and 4c), for others, this correlation does not exist or there is not

enough mineral/chemical data to test for a relationship. VIS-NIR absorption strength is expected to be nonlinearly related to composition (e.g., Van de Hulst 1981; Hapke 1993), and only a few other studies have looked at absorption strength and composition for comparable materials (Garenne et al. 2016; Kaplan et al. 2019). In all likelihood, obtaining more than relative abundances from the mineral/chemical maps produced using these indices will be a nontrivial task.

The potential also exists for data with low signal-to-noise ratios or spikes at specific wavelengths to influence the Spindex band depths (and specifically band depths above the determined threshold value). For some indices (e.g., organics and other weaker features), absorptions may only be detected below the given threshold value, and individual spectra will need to be visually inspected to distinguish between noise and spectral features at these low values. Similarly, absorption features in regions where there are multiple similar absorptions (e.g., the 1  $\mu\text{m}$  feature in both olivine and pyroxene) will be difficult to distinguish with spectral indices. Combinations of bands may be needed to positively detect these phases (e.g., checking whether the 2  $\mu\text{m}$  band is present to potentially distinguish pyroxene from olivine). We recommend that any important or unusual identifications, and especially any band depths with high uncertainty values, should be validated manually in the original spectral data before inclusion or exclusion from maps.

Although we attempted to create a comprehensive set of spectral indices, asteroid and/or instrument conditions may require additional indices or adjustment of existing ones. The laboratory spectra used to test the indices typically were measured under ambient conditions that may have led to the observation of hydration features not indigenous to the samples. Additionally, indices that are deemed inappropriate for C chondrites or carbonaceous asteroids may be highly useful for other applications.

Space weathering, in particular, will change spectral features in ways that are not readily testable with unweathered samples in our spectral libraries. In addition to the spectral indices discussed here, we will assess slopes for multiple regions of the OVIRS spectrum as a measure of space weathering (Lantz et al. 2015, 2017). Differences in slopes and absorption-feature strength and shape, when taken in the context of geologic observations, will inform our understanding of space weathering on Bennu.

### PRELIMINARY RESULTS FROM BENNU

The first disk-integrated VNIR spectrum of Bennu has a blue slope, consistent with ground observations, and a distinct “3  $\mu\text{m}$ ” band (Hamilton et al. 2019;



Fig. 6). When Spindex is applied to that spectrum, only three spectral indices (#3, 4, and 52) have band depths > 5%. All three indices are associated with the “3  $\mu\text{m}$ ” band, and band depths between 16% and 18% are recorded depending on the position of the band center. The spectral index centered at 2.7  $\mu\text{m}$  (#7) is located shortward of Bennu’s  $\sim 2.74\text{-}\mu\text{m}$  band center (Hamilton et al. 2019) and therefore remains <5%. We observe no other absorption features in this spectrum, and no false positives are reported with Spindex. Disk-integrated spectra, by their nature, are commonly not representative of what is observed at high spatial resolution (e.g., Hubble Mars versus CRISM Mars). Future, spatially resolved spectra could exhibit greater variation and all will be run through Spindex.

## CONCLUSIONS

From 95 spectral indices derived from the literature, we describe the 17 that are most likely to capture the mineral and chemical diversity on Bennu and in C chondrite meteorites (Table 3). We tested these indices on 1149 mineral spectra and 293 meteorite spectra. They (1) identify absorption features that we expect to be present on Bennu and (2) rarely falsely identify absorptions that are not present in the spectrum. In the course of finding the best indices, we also identified indices that routinely return negative and/or false results, which require caution when applied to asteroid or meteorite spectra. Although the laboratory spectra do not show systematic relationships between albedo or particle size and band depth, we anticipate that differences in albedo, particle size, viewing geometry, temperature, and space weathering could have a discernable effect on the spectra gathered at Bennu.

These results will provide guidelines for mineral/chemical mapping on Bennu. Global and local mineral/chemistry maps at <50 m spatial resolution will be used in the selection and characterization of a primary sample site on Bennu. Preliminary analysis of Bennu’s spectrum with Spindex detects a 3  $\mu\text{m}$  absorption, and no other spectral features. As illustrated by the C chondrites spectra, the combination of weak absorptions and an absorbing matrix can make it difficult to use spectral indices alone to understand the complex mineralogy of a body like Bennu and additional spectral interpretation will be needed in addition to the indices. However, this set of tested indices may serve as a guideline for future mapping of carbonaceous asteroids or meteorites, particularly where the amount of data collected makes parameterization desirable. The metrics used in this study to determine confidence level in each spectral index (e.g., positive and false positive detection rates calculated for various minerals and meteorite groups) will be useful

for estimating errors on the mineral/chemical maps when considered alongside instrument and observation conditions. The sample returned by the mission will ultimately test our spectral interpretations of the composition of Bennu’s surface.

*Acknowledgments*—This material is based on work supported by NASA under Contract NNM10AA11C issued through the New Frontiers Program. We are grateful to the entire OSIRIS-REx Team for making the encounter with Bennu possible. J.B.R. and E.D. were supported for this research by the Italian Space Agency (ASI) under the ASI-INAF agreement no. 2017-37-H.0.

*Editorial Handling*—Dr. Carle Pieters

## REFERENCES

- Abreu N. M. and Brearley A. J. 2010. Early solar system processes recorded in the matrices of two highly pristine CR3 carbonaceous chondrites, MET 00426 and QUE 99177. *Geochimica et Cosmochimica Acta* 74:1146–1171.
- Adams J. B. 1974. Visible and near-infrared diffuse reflectance spectra of pyroxenes as applied to remote sensing of solid objects in the solar system. *Journal of Geophysical Research* 79:4829–4836.
- Alexander C. M. O’D., Fogel M., Yabuta H., and Cody G. D. 2007. The origin and evolution of chondrites recorded in the elemental and isotopic compositions of their macromolecular organic matter. *Geochimica et Cosmochimica Acta* 71:4380–4403.
- Alexander C. M. O’D., Bowden R., Fogel M. L., and Howard K. T. 2015. Carbonate abundances and isotopic compositions in chondrites. *Meteoritics & Planetary Science* 50:810–833.
- Alexander C. M. O’D., Cody G. D., De Gregorio B. T., Nittler L. R., and Stroud R. M. 2017. The nature, origin and modification of insoluble organic matter in chondrites, the major source of Earth’s C and N. *Chemie der Erde—Geochemistry* 77:227–256.
- Ammannito E., DeSanctis M. C., Ciarniello M., Frigeri A., Carozzo F. G., Combe J.-P., Ehlmann B. L., Marchi S., McSween H. Y., Raponi A., Toplis M. J., Tosi F., Castillo-Rogez J. C., Capaccioni F., Capria M. T., Fonte S., and Giardino M. 2016. Distribution of phyllosilicates on the surface of Ceres. *Science* 353:aaf4279.
- Beck P., Quirico E., Montes-Hernandez G., Bonal L., Bollard J., Orthous-Daunay F.-R., Howard K. T., Schmitt B., Brissaud O., Deschamps F., Wundere B., and Guillot S. 2010. Hydrous mineralogy of CM and CI chondrites from infrared spectroscopy and their relationship with low albedo asteroids. *Geochimica et Cosmochimica Acta* 74:4881–4892.
- Beck P., Garenne A., Quirico E., Bonal L., Montes-Hernandez G., Moynier F., and Schmitt B. 2014. Transmission infrared spectra (2–25  $\mu\text{m}$ ) of carbonaceous chondrites (CI, CM, CV–CK, CR, C2 ungrouped): Mineralogy, water, and asteroidal processes. *Icarus* 229:263–277.
- Beck P., Maturilli A., Garenne A., Vernazza P., Helbert J., Quirico E., and Schmitt B. 2018. What is controlling the



- reflectance spectra (0.35–150  $\mu\text{m}$ ) of hydrated (and dehydrated) carbonaceous chondrites? *Icarus* 313:124–138.
- Bell J. F., Bell J. F., McSween H. Y., Crisp J. A., Morris R. V., Murchie S. L., Bridges N. T., Johnson J. R., Britt D. T., Golombek M. P., Moore H. J., Ghosh A., Bishop J. L., Anderson R. C., Brückner J., Economou T., Greenwood J. P., and Gunnlaugsson H. 2000. Mineralogic and compositional properties of Martian soil and dust: Results from Mars Pathfinder. *Journal of Geophysical Research: Planets* 105:1721–1755.
- Berkley J. L., Taylor G. J., Keil K., Harlow G. E., and Prinz M. 1980. The nature and origin of ureilites. *Geochimica et Cosmochimica Acta* 44:1579–1597.
- Bevington P. R. 1969. *Data reduction and error analysis for the physical sciences*. New York: McGraw-Hill. <https://books.google.com/books?id=999QAAAAMAAJ>.
- Binzel R. P., DeMeo F. E., Burt B. J., Cloutis E. A., Rozitis B., Burbine T. H., Campins H., Clark B. E., Emery J. P., Hergenrother C. W., Howell E. S., Lauretta D. S., Nolan M. C., Mansfield M., Pietrasz V., Polishook D., and Scheeres D. J. 2015. Spectral slope variations for OSIRIS-REx target Asteroid (101955) Bennu: Possible evidence for a fine-grained regolith equatorial ridge. *Icarus* 256:22–29.
- Bishop J. L. and Pieters C. M. 1995. Low-temperature and low atmospheric pressure infrared reflectance spectroscopy of Mars soil analog materials. *Journal of Geophysical Research* 100:5369.
- Bland P. A., Cressey G., and Menzies O. N. 2004. Modal mineralogy of carbonaceous chondrites by X-ray diffraction and Mössbauer spectroscopy. *Meteoritics & Planetary Science* 39:3–16.
- Bossa J.-B., Duvernay F., Theulé P., Borget F., d'Hendecourt L., and Chiavassa T. 2009. Methylammonium methylcarbamate thermal formation in interstellar ice analogs: A glycine salt precursor in protostellar environments. *Astronomy & Astrophysics* 506:601–608.
- Bottke W. F., Bottke W. F., Vokrouhlický D. Y., Walsh K. J., Delbo M., Michel P., Lauretta D. S., Campins H., Connolly H. C. Jr., Scheeres D. J., and Chelsey S. R. 2015. In search of the source of asteroid (101955) Bennu: Applications of the stochastic YORP model. *Icarus* 247:191–217.
- Browning L. B., McSween H. Y., and Zolensky M. E. 1996. Correlated alteration effects in CM carbonaceous chondrites. *Geochimica et Cosmochimica Acta* 60:2621–2633.
- Campins H., Hargrove K., Pinilla-Alonso N., Howell E. S., Kelley M. S., Licandro J., Mothé-Diniz T., Fernández Y., and Ziffer J. 2010. Water ice and organics on the surface of the asteroid 24 Themis. *Nature* 464:1320–1321.
- Campins H., León J. de, Licandro J., Hendrix A., Sánchez J. A., and Ali-Lagoa V. 2018. Compositional diversity among primitive asteroids. In *Primitive meteorites and asteroids*, edited by Abreu N. San Diego, California: Elsevier. pp. 345–369.
- Capaccioni F., Capaccioni F., Coradini A., Filacchione G., Erard S., Arnold G., Drossart P., De Sanctis M. C., Bockelee-Morvan D., Capria M. T., Tosi F., Leyrat C., Schmitt B., Quirico E., Cerroni P., Mennella V., Raponi A., Ciarniello M., and McCord T. 2015. The organic-rich surface of comet 67P/Churyumov-Gerasimenko as seen by VIRTIS/Rosetta. *Science* 347:aaa0628.
- Cataldo F., García-Hernández D. A., and Manchado A. 2013. Far- and mid-infrared spectroscopy of complex organic matter of astrochemical interest: Coal, heavy petroleum fractions and asphaltene. *Monthly Notices of the Royal Astronomical Society* 429:3025–3039.
- Chiar J. E., Tielens A. G. G. M., Adamson A. J., and Ricca A. 2013. The structure, origin, and evolution of interstellar hydrocarbon grains. *The Astrophysical Journal* 770:78.
- Christensen P. R., Hamilton V. E., Mehall G. L., Pelham D., O'Donnell W., Anwar S., Bowles H., Chase S., Fahlgren J., Farkas Z., Fisher T., James O., Kubik I., Lazbin I., Miner M., Rassas M., Schulze L., Shamordola K., Tourville T., West G., Woodward R., and Lauretta D. 2018. The OSIRIS-REx thermal emission spectrometer (OTES) instrument. *Space Science Reviews* 214:87.
- Clark B. E., Ziffer J., Nesvorný D., Campins H., Rivkin A., Hiroi T., Barucci M. A., Binzel R., Fornasier S., DeMeo F., and Ockert-Bell M. 2010. Spectroscopy of B-type asteroids: Subgroups and meteorite analogs. *Journal of Geophysical Research* 115, E06005. <https://doi.org/doi.wiley.com/10.1029/2009je003478>
- Clark B. E., Binzel R. P., Howell E. S., Cloutis E. A., Ockert-Bell M., Christensen M. P., Antonietta Barucci M., DeMeo F., Lauretta D. S., Connolly H. Jr., Soderberg A., Hergenrother C., Lim L., Emery J., and Mueller M. 2011. Asteroid (101955) 1999 RQ36: Spectroscopy from 0.4 to 2.4  $\mu\text{m}$  and meteorite analogs. *Icarus* 216:462–475.
- Clark R. N. 1983. Spectral properties of mixtures of montmorillonite and dark carbon grains: Implications for remote sensing minerals containing chemically and physically adsorbed water. *Journal of Geophysical Research* 88:10,635.
- Clark R. N. and Roush T. L. 1984. Reflectance spectroscopy: Quantitative analysis techniques for remote sensing applications. *Journal of Geophysical Research* 89:6329–6340.
- Clark R. N., King T. V. V., Klejwa M., Swayze G. A., and Vergo N. 1990. High spectral resolution reflectance spectroscopy of minerals. *Journal of Geophysical Research* 95:12,653.
- Clark R. N. 1999. Spectroscopy of rocks and minerals, and principles of spectroscopy. In *Manual of remote sensing, volume 3, remote sensing for the earth sciences*, edited by Rencz A. N. New York: John Wiley and Sons. pp. 3–58.
- Cloutis E. A., Sunshine J. M., and Morris R. V. 2004. Spectral reflectance-compositional properties of spinels and chromites: Implications for planetary remote sensing and geothermometry. *Meteoritics & Planetary Science* 39:545–565.
- Cloutis E., Hawthorne F. C., Mertzman S. A., Krenna K., Craig M. A., Marcino D., Methot M., Strong J., Mustard J. F., Blaney D. L., Bell J. F. III, and Vilas F. 2006. Detection and discrimination of sulfate minerals using reflectance spectroscopy. *Icarus* 184:121–157.
- Cloutis E. A., Hiroi T., Gaffey M. J., Alexander C. M. O., and Mann P. 2011a. Spectral reflectance properties of carbonaceous chondrites: 1. CI chondrites. *Icarus* 212:180–209.
- Cloutis E. A., Hudon P., Hiroi T., Gaffey M. J., and Mann P. 2011b. Spectral reflectance properties of carbonaceous chondrites: 2 CM chondrites. *Icarus* 216:309–346.
- Dartois E., Muñoz Caro G. M., Deboffe D., and d'Hendecourt L. 2004. Diffuse interstellar medium organic polymers: Photoproduction of the 3.4, 6.85 and 7.25  $\mu\text{m}$  features. *Astronomy & Astrophysics* 423:L33–L36.
- De León J., Campins H., Morate D., Pr Deá M., Ali-Lagoa V., Licandro J., Rizos J. L., Pinilla-Alonso N., DellaGiustina

- D. N., Lauretta D. S., Popescu M., and Lorenzi V. 2018. Expected spectral characteristics of (101955) Bennu and (162173) Ryugu, targets of the OSIRIS-REx and Hayabusa2 missions. *Icarus* 313:25–37.
- De Sanctis M. C., De Sanctis M. C., Ammannito E., McSween H. Y., Raponi A., Marchi S., Capaccioni F., Capria M. T., Carrozzo F. G., Ciarniello M., Fonte S., Formisano M., Frigeri A., Giardino M., Longobardo A., Magni G., McFadden L. A., and Palomba E. C. 2017. Localized aliphatic organic material on the surface of Ceres. *Science* 355:719–722.
- Donaldson Hanna K. L., Schrader D. L., Cloutis E. A., Cody G. D., King A. J., McCoy T. J., Applin D. M., Mann J. P., Bowles N. E., Brucato J. R., Connolly H. C. Jr, Dotto E., Keller L. P., Lim L. F., Clark B. E., Hamilton V. E., Lantz C., Lauretta D. S., Russell S. S., and Schofield P. F. 2019. Spectral characterization of analog samples in anticipation of OSIRIS-REx's arrival at Bennu: A blind test study. *Icarus* 319:701–723.
- Duley W. W. and Williams D. A. 1981. The infrared spectrum of interstellar dust: Surface functional groups on carbon. *Monthly Notices of the Royal Astronomical Society* 196:269–274.
- Feaga L. M., A'Hearn M. F., Sunshine J. M., Groussin O., and Farnham T. L. 2007. Asymmetries in the distribution of H<sub>2</sub>O and CO<sub>2</sub> in the inner coma of Comet 9P/Tempel 1 as observed by Deep Impact. *Icarus* 191:134–145.
- Garenne A., Beck P., Montes-Hernandez G., Brissaud O., Schmitt B., Quirico E., Bonal L., Beck C., and Howard K. T. 2016. Bidirectional reflectance spectroscopy of carbonaceous chondrites: Implications for water quantification and primary composition. *Icarus* 264:172–183.
- Gerakines P. A., Hudson R. L., Moore M. H., and Bell J.-L. 2012. In situ measurements of the radiation stability of amino acids at 15–140K. *Icarus* 220:647–659.
- Grundy W. M. and Schmitt B. 1998. The temperature-dependent near-infrared absorption spectrum of hexagonal H<sub>2</sub>O ice. *Journal of Geophysical Research: Planets* 103:25,809–25,822.
- Hamilton V. E., Simon A. A., Christensen P. R., Reuter D. C., Clark B. E., Barucci M. A., Bowles N. E., Boynton W. V., Brucato J. R., Cloutis E. A., Connolly H. C. Jr, Donaldson Hanna K. L., Emery J. P., Enos H. L., Fornasier S., Haberle C. W., Hanna R. D., Howell E. S., Kaplan H. H., Keller L. P., Lantz C., Li J.-Y., Lim L. F., McCoy T. J., Merlin F., Nolan M. C., Praet A., Rozitis B., Sandford S. A., Schrader D. L., Thomas C. A., Zou X.-D., and Lauretta D. S.; the OSIRIS-REx Team. 2019. Evidence for widespread hydrated minerals on asteroid (101955) Bennu. *Nature Astronomy*, 3:332–340.
- Hapke B. 1993. *Theory of reflectance and emittance spectroscopy*. Cambridge, UK: Cambridge University Press.
- Hiroi T., Zolensky M. E., Pieters C. M., and Lipschutz M. E. 1996. Thermal metamorphism of the C, G, B, and F asteroids seen from the 0.7  $\mu$ m, 3  $\mu$ m, and UV absorption strengths in comparison with carbonaceous chondrites. *Meteoritics & Planetary Science* 31:321–327.
- Howard K. T., Benedix G. K., Bland P. A., and Cressey G. 2009. Modal mineralogy of CM2 chondrites by X-ray diffraction (PSD-XRD). Part 1: Total phyllosilicate abundance and the degree of aqueous alteration. *Geochimica et Cosmochimica Acta* 73:4576–4589.
- Howard K. T., Alexander C. M. O., Schrader D. L., and Dyl K. A. 2015. Classification of hydrous meteorites (CR, CM and C2 ungrouped) by phyllosilicate fraction: PSD-XRD modal mineralogy and planetesimal environments. *Geochimica et Cosmochimica Acta* 149:206–222.
- Hudgins D. M., Sandford S. A., Allamandola L. J., and Tielens A. G. G. M. 1993. Mid- and far-infrared spectroscopy of ices—Optical constants and integrated absorbances. *The Astrophysical Journal Supplement Series* 86:713.
- Johnson T. V. and Fanale F. P. 1973. Optical properties of carbonaceous chondrites and their relationship to asteroids. *Journal of Geophysical Research* 78:8507–8518.
- Kaplan H. H. and Milliken R. E. 2018. Reflectance spectroscopy of organic matter in sedimentary rocks at visible-mid-infrared wavelengths. *Clays and Clay Minerals*, 66:173–189. <http://www.ingentaconnect.com/content/10.1346/CCMN.2018.064092>.
- Kaplan H. H., Milliken R. E., and Alexander C. M. O'D. 2018. New constraints on the abundance and composition of organic matter on Ceres. *Geophysical Research Letters* 45:5274–5282.
- Kaplan H. H., Milliken R. E., Alexander C. M. O'D., and Herd C. D. K. 2019. Reflectance spectroscopy of insoluble organic matter (IOM) and carbonaceous meteorites. *Meteoritics & Planetary Science* 54:1051–1068. doi:<http://doi.wiley.com/10.1111/maps.13264>.
- Kebukawa Y., Alexander C. M. O'D., and Cody G. D. 2011. Compositional diversity in insoluble organic matter in type 1, 2 and 3 chondrites as detected by infrared spectroscopy. *Geochimica et Cosmochimica Acta*. 75:3530–3541.
- King A. J., Schofield P. F., Howard K. T., and Russell S. S. 2015. Modal mineralogy of CI and CI-like chondrites by X-ray diffraction. *Geochimica et Cosmochimica Acta* 165:148–160.
- King T. V. V. and Clark R. N. 1989. Spectral characteristics of chlorites and Mg-serpentines using high-resolution reflectance spectroscopy. *Journal of Geophysical Research: Solid Earth* 94:13,997–14,008.
- King T. V. V. and Ridley W. I. 1987. Relation of the spectroscopic reflectance of olivine to mineral chemistry and some remote sensing implications. *Journal of Geophysical Research* 92:11457–11469.
- Lantz C., Brunetto R., Barucci M. A., Dartois E., Duprat J., Engrand C., Godard M., Ledu D., and Quirico E. 2015. Ion irradiation of the Murchison meteorite: Visible to mid-infrared spectroscopic results. *Astronomy & Astrophysics* 577:A41.
- Lantz C., Brunetto R., Barucci M. A., Fornasier S., Baklouti D., Bourçois J., and Godard M. 2017. Ion irradiation of carbonaceous chondrites: A new view of space weathering on primitive asteroids. *Icarus* 285:43–57.
- Lauretta D. S., Hua X., and Buseck P. R. 2000. Mineralogy of fine-grained rims in the alh 81002 cm chondrite. *Geochimica et Cosmochimica Acta* 64:3263–3273.
- Lauretta D. S., Bartels A. E., Barucci M. A., Bierhaus E. B., Binzel R. P., Bottke W. F., Campins H., Chesley S. R., Clark B. C., Clark B. E., Cloutis E. A., Connolly H. C., Crombie M. K., Delb M. Ó, Dworkin J. P., Emery J. P., Glavin D. P., and Hamilton V. E. 2015. The OSIRIS-REx target asteroid (101955) Bennu: Constraints on its physical, geological, and dynamical nature from astronomical observations. *Meteoritics & Planetary Science* 50:834–849.
- Lebofsky L. A. 1980. Infrared reflectance spectra of asteroids—A search for water of hydration. *The Astronomical Journal* 85:573.

- Lucey P. G., Taylor G. J., and Malaret E. 1995. Abundance and distribution of iron on the Moon. *Science* 268:1150–1153.
- Mastrapa R. M., Sandford S. A., Roush T. L., Cruikshank D. P., Dalle Ore C. M. 2009. Optical constants of amorphous and crystalline H<sub>2</sub>O -ice: 2.5 - 22 μm (400–455 cm<sup>-1</sup>) optical constants of H<sub>2</sub>O -ice. *The Astrophysical Journal* 701:1347–1356.
- McGuire A. and Hapke B. 1995. An experimental study of light scattering by large, irregular particles. *Icarus* 113:134–155.
- McSween H. Y. 1977. On the nature and origin of isolated olivine grains in carbonaceous chondrites. *Geochimica et Cosmochimica Acta* 41:411–418.
- Merlin F., Quirico E., Barucci M. A., and de Bergh C. 2012. Methanol ice on the surface of minor bodies in the solar system. *Astronomy & Astrophysics* 544:A20.
- Merouane S., Djouadi Z., d'Hendecourt L. L. S., Zanda B., and Borg J. 2012. Hydrocarbon materials of likely interstellar origin from the Paris meteorite. *The Astrophysical Journal* 756:154.
- Michalski J., Poulet F., Bibring J.-P., and Mangold N. 2010. Analysis of phyllosilicate deposits in the Nili Fossae region of Mars: Comparison of TES and OMEGA data. *Icarus* 206:269–289.
- Milliken R. and Mustard J. 2007. Estimating the water content of hydrated minerals using reflectance spectroscopy I. Effects of darkening agents and low-albedo materials. *Icarus* 189:550–573.
- Moroz L. V., Arnold G., Korochantsev A. V., and Wäsch R. 1998. Natural solid bitumens as possible analogs for cometary and asteroid organics. *Icarus* 134:253–268.
- Murchie S. 2000. Near-infrared spectral variations of martian surface materials from ISM imaging spectrometer data. *Icarus* 147:444–471.
- Murchie S., Roach L., Seelos F., Milliken R., Mustard J., Arvidson R., Wiseman S., Lichtenberg K., Hanna J. A., Bishop J., Bibring P., Parente M., and Morris R. 2009. Evidence for the origin of layered deposits in Candor Chasma, Mars, from mineral composition and hydrologic modeling. *Journal of Geophysical Research* 114:E00D05. <https://doi.org/doi.wiley.com/10.1029/2009je003343>
- Mustard J. and Hays J. 1997. Effects of hyperfine particles on reflectance spectra from 0.3 to 25 μm. *Icarus* 125:145–163.
- Nash D. B. and Conel J. E. 1974. Spectral reflectance systematics for mixtures of powdered hypersthene, labradorite, and ilmenite. *Journal of Geophysical Research* 79:1615–1621.
- Ody A., Poulet F., Langevin Y., Bibring J.-P., Bellucci G., Altieri F., Gondet B., Vincendon M., Carter J., and Manau N. 2012. Global maps of anhydrous minerals at the surface of Mars from OMEGA/MEx. *Journal of Geophysical Research: Planets* 117:n/a–n/a.
- Ody A., Poulet F., Bibring J.-P., Loizeau D., Carter J., Gondet B., and Langevin Y. 2013. Global investigation of olivine on Mars: Insights into crust and mantle compositions. *Journal of Geophysical Research: Planets* 118:234–262.
- Orthous-Daunay F.-R., Quirico E., Beck P., Brissaud O., Dartois E., Pino T., and Schmitt B. 2013. Mid-infrared study of the molecular structure variability of insoluble organic matter from primitive chondrites. *Icarus* 223:534–543.
- Pelkey S. M., Mustard J. F., Murchie S., Clancy R. T., Wolff M., Smith M., Milliken R. J., Bibring P., Gendrin A., Poulet F., Langevin Y., and Gondet B. 2007. CRISM multispectral summary products: Parameterizing mineral diversity on Mars from reflectance. *Journal of Geophysical Research* 112:E08S14. <https://doi.org/doi.wiley.com/10.1029/2006je002831>.
- Pendleton Y. J. and Allamandola L. J. 2002. The organic refractory material in the diffuse interstellar medium: Mid-infrared spectroscopic constraints. *The Astrophysical Journal Supplement Series* 138:75–98.
- Reuter D. C., Simon A. A., Hair J., Lunsford S., Manthripragada S., Bly V., Bos B., Brambora C., Caldwell E., Casto G., Dolch Z., Finneran P., Jennings D., Jhabvala D., Matson E., McLelland M., Roher W., Sullivan T., Weigle E., Wen Y., Wilson D., and Lauretta S. 2018. The OSIRIS-REx visible and infrared spectrometer (OVIRS): Spectral maps of the asteroid Bennu. *Space Science Reviews* 214:54.
- Rivkin A. 2002. Hydrated minerals on asteroids: The astronomical record. *Asteroids III* 1:235–253.
- Rivkin A. S. and Emery J. P. 2010. Detection of ice and organics on an asteroidal surface. *Nature* 464:1322–1323.
- Schmitt-Kopplin P., Gabelica Z., Gougeon R. D., Fekete A., Kanawati B., Harir M., Gebefuegi I., Eckel G., and Hertkorn N. 2010. High molecular diversity of extraterrestrial organic matter in Murchison meteorite revealed 40 years after its fall. *Proceedings of the National Academy of Sciences* 107:2763–2768.
- Sheng Y. J., Hutcheon I. D., and Wasserburg G. J. 1991. Origin of plagioclase-olivine inclusions in carbonaceous chondrites. *Geochimica et Cosmochimica Acta* 55:581–599.
- Simon A., Reuter D., Gorius N., Lunsford A., Cosentino R., Wind G., and Lauretta D. and the OSIRIS-REx Team. 2018. In-flight calibration and performance of the OSIRIS-REx Visible and IR Spectrometer (OVIRS). *Remote Sensing* 10:1486.
- Sunshine J. M., Farnham T. L., Feaga L. M., Groussin O., Merlin F., Milliken R. E., and A'Hearn M. F. 2009. Temporal and spatial variability of lunar hydration as observed by the deep impact spacecraft. *Science* 326:565–568.
- Takir D. and Emery J. P. 2012. Outer Main Belt asteroids: Identification and distribution of four 3-μm spectral groups. *Icarus* 219:641–654.
- Takir D., Emery J. P., McSween H. Y., Hibbitts C. A., Clark R. N., Pearson N., and Wang A. 2013. Nature and degree of aqueous alteration in CM and CI carbonaceous chondrites. *Meteoritics & Planetary Science*. 48:1618–1637.
- Takir D., Emery J. P., and McSween H. Y. 2015. Toward an understanding of phyllosilicate mineralogy in the outer main asteroid belt. *Icarus* 257:185–193.
- Takir D., Stockstill-Cahill K. R., Hibbitts C. A., and Nakauchi Y. 2019. 3-μm reflectance spectroscopy of carbonaceous chondrites under asteroid-like conditions. *Icarus* 333:243–251.
- Thollot P., Mangold N., Ansan V., Le Mouélic S., Milliken R. E., Bishop J. L., Weitz C. M., Roach L. H., Mustard J. F., and Murchie S. L. 2012. Mars most minerals in a nutshell: Various alteration phases formed in a single environment in Labyrinthus Noctis. *Journal of Research Geophysical: Planets* 117.
- Thompson M. S., Loeffler M. J., Morris R. V., Keller L. P., and Christoffersen R. 2019. Spectral and chemical effects of simulated space weathering of the Murchison CM2 carbonaceous chondrite. *Icarus* 319:499–511.

- Tomeoka K. and Buseck P. R. 1988. Matrix mineralogy of the Orgueil CI carbonaceous chondrite. *Geochimica et Cosmochimica Acta* 52:1627–1640.
- Van de Hulst H. C. 1981. *Light scattering by small particles*. New York: Dover Publications.
- Vilas F. 1994. A cheaper, faster, better way to detect water of hydration on solar system bodies. *Icarus* 111:456–467.
- Vilas F. and Gaffey M. J. 1989. Phyllosilicate absorption features in main-belt and outer-belt asteroid reflectance spectra. *Science* 246:790–792.
- Viviano-Beck C. E., Seelos F. P., Murchie S. L., Kahn E. G., Seelos K. D., Taylor H. W., Taylor K., Ehlmann B. L., Wiseman S. M., Mustard J. F., and Frank Morgan M. 2014. Revised CRISM spectral parameters and summary products based on the currently detected mineral diversity on Mars. *Journal of Geophysical Research: Planets* 119:1403–1431.
- Walsh K. J., Delbó M., Bottke W. F., Vokrouhlický D., and Lauretta D. S. 2013. Introducing the Eulalia and new Polana asteroid families: Re-assessing primitive asteroid families in the inner Main Belt. *Icarus* 225:283–297.
- Wray J. J., Ehlmann B. L., Squyres S. W., Mustard J. F., and Kirk R. L. 2008. Compositional stratigraphy of clay-bearing layered deposits at Mawrth Vallis, Mars. *Geophysical Research Letters* 35.
- Zolensky M., Barrett R., and Browning L. 1993. Mineralogy and composition of matrix and chondrule rims in carbonaceous chondrites. *Geochimica et Cosmochimica Acta* 57:3123–3148.

## SUPPORTING INFORMATION

Additional supporting information may be found in the online version of this article.

**Fig. S1.** These plots show the equations used to compute spectral indices in Spindex. Example spectra and wavelengths are depicted in relation to these equations.

**Fig. S2.** The band depth at 3  $\mu\text{m}$  for the 293 meteorite spectra. Symbols designate different kinds of samples (i.e. chips, particulates) and spectral measurement conditions (i.e. ambient, vacuum). As expected, the vacuum spectra have weaker band depths and a larger portion of the samples have a 3  $\mu\text{m}$  absorption below the detection limit (0.05, blue line).

**Fig. S3.** Meteorite spectra used in this study, normalized at 0.55  $\mu\text{m}$  and offset in order to display spectral shape. One additional set of C chondrite spectra taken under vacuum are plotted and discussed in Takir et al. (2013, 2015).

**Table S1.1.1–1.13.** Positive and false positive results for all mineral and meteorite spectra. The first 12 tables represent compositional groupings of parameters (those targeting carbonates, hydrated minerals, etc.). The final table has meteorite positives and false positives for all parameters. The positive detection rate is broken down by mineral or meteorite group. The false detection rate is for all mineral or all meteorite spectra.

---